JEM Journal of Experimental Medicine

ARTICLE

Trapping of CDC42 C-terminal variants in the Golgi drives pyrin inflammasome hyperactivation

Masahiko Nishitani-Isa[1]*, Kojiro Mukai[2]*, Yoshitaka Honda[1,3,4], Hiroshi Nihira[1], Takayuki Tanaka[1], Hirofumi Shibata[1], Kumi Kodama[1], Eitaro Hiejima[1], Kazushi Izawa[1], Yuri Kawasaki[5], Mitsujiro Osawa[5], Yu Katata[6], Sachiko Onodera[6], Tatsuya Watanabe[6], Takashi Uchida[7], Shigeo Kure[7], Junko Takita[1], Osamu Ohara[8], Megumu K. Saito[5], Ryuta Nishikomori[9], Tomohiko Taguchi[2], Yoji Sasahara[7], and Takahiro Yasumi[1]

Mutations in the C-terminal region of the *CDC42* gene cause severe neonatal-onset autoinflammation. Effectiveness of IL-1β–blocking therapy indicates that the pathology involves abnormal inflammasome activation; however, the mechanism underlying autoinflammation remains to be elucidated. Using induced-pluripotent stem cells established from patients carrying CDC42^{R186C}, we found that patient-derived cells secreted larger amounts of IL-1β in response to pyrin-activating stimuli. Aberrant palmitoylation and localization of CDC42^{R186C} protein to the Golgi apparatus promoted pyrin inflammasome assembly downstream of pyrin dephosphorylation. Aberrant subcellular localization was the common pathological feature shared by CDC42 C-terminal variants with inflammatory phenotypes, including CDC42^{*192C*24} that also localizes to the Golgi apparatus. Furthermore, the level of pyrin inflammasome overactivation paralleled that of mutant protein accumulation in the Golgi apparatus, but not that of the mutant GTPase activity. These results reveal an unexpected association between CDC42 subcellular localization and pyrin inflammasome activation that could pave the way for elucidating the mechanism of pyrin inflammasome formation.

Introduction

Autoinflammatory disorders are caused by dysregulated activation of innate immune systems and typically present in early childhood with fever and disease-specific patterns of organ inflammation. The concept of autoinflammatory diseases was proposed in 1999, and since that time a growing number of genetic causes have been identified for a variety of diseases (Manthiram et al., 2017; McDermott et al., 1999). Disease-based research has revealed the molecular mechanisms of excessive innate immune responses that drive autoinflammatory phenotypes, and these discoveries have provided us with novel therapeutic targets that might be used to effectively treat these conditions (Nigrovic et al., 2020).

C-terminal variants of cell division control protein 42 homolog (CDC42) were recently shown to cause severe inflammation that presents in the neonatal period with fever, rashes, and a significant increase in inflammatory markers, culminating in the development of hemophagocytic lymphohistiocytosis (HLH; Bekhouche et al., 2020; Gernez et al., 2019; Lam et al., 2019). Among the three reported variants (c.556C>T, *CDC42^{R186C}*; c.563G>A, *CDC42^{C188Y}*; c.576A>C, *CDC42^{*192C*24}*), *CDC42^{R186C}* induces the most severe phenotype. A unique property of CDC42^{R186C} is its aberrant localization to the Golgi apparatus, and previous studies suggested that impaired natural killer (NK) cell function or enhanced NF-κB signaling are associated with inflammation in the patients (Bekhouche et al., 2020; Lam et al., 2019). However, effectiveness of IL-1β blocking reagents indicates that activation of an inflammasome is central to pathogenesis.

Studies of autoinflammatory pathology in humans have often been hampered by the limited availability of patient samples. To overcome this difficulty, we used induced-pluripotent stem cells (iPSCs) established from the patients (Saito, 2021). iPSC-derived myeloid cell lines (iPS-MLs) can be obtained by introducing three transgenes into iPSC-derived monocytes (Kawasaki et al., 2017). iPS-MLs phenotypically and functionally resemble primary immature macrophages and can be expanded in the

[1]Department of Pediatrics, Kyoto University Graduate School of Medicine, Kyoto, Japan; [2]Department of Integrative Life Sciences, Graduate School of Life Sciences, Tohoku University, Sendai, Japan; [3]Institute for the Advanced Study of Human Biology (ASHBi), Kyoto University, Kyoto, Japan; [4]Department of Immunology, Kyoto University Graduate School of Medicine, Kyoto, Japan; [5]Department of Clinical Application, Center for iPS Cell Research and Application, Kyoto University, Kyoto, Japan; [6]Department of Neonatology, Miyagi Children's Hospital, Sendai, Japan; [7]Department of Pediatrics, Tohoku University Graduate School of Medicine, Sendai, Japan; [8]Department of Applied Genomics, Kazusa DNA Research Institute, Kisarazu, Japan; [9]Department of Pediatrics, Kurume University Graduate School of Medicine, Kurume, Japan.

*M. Nishitani-Isa and K. Mukai contributed equally to this paper. Correspondence to Takahiro Yasumi: yasumi@kuhp.kyoto-u.ac.jp; Yoji Sasahara: ysasahara@med.tohoku.ac.jp.

presence of M-CSF. iPS-MLs can fully differentiate into macrophages (iPS-MPs), which produce higher levels of IL-1β and IL-18. These cell lines are useful for studying human autoinflammatory disorders, especially for analyses of the pyrin inflammasome. By contrast, it is difficult to establish a mouse disease model because murine pyrin lacks the B30.2/SPRY domain, where most mutations are associated with familial Mediterranean fever (FMF) cluster (Chae et al., 2011).

In this study, we established iPS-MLs and iPS-MPs from patients carrying the *CDC42*^{R186C} mutation and demonstrated that the pyrin inflammasome plays an important role in driving hyperinflammation.

Results

CDC42^{R186C} triggers aberrant activation of pyrin inflammasome

Continuous elevation of IL-18 in the sera of the two patients with the *CDC42*^{R186C} variant (Fig. S1), along with previous reports describing a therapeutic benefit of anti–IL-1β treatment (Gernez et al., 2019; Lam et al., 2019), suggested that inflammasome activation is central to the pathogenesis of *CDC42*-associated autoinflammation. To determine whether a specific inflammasome is overactivated in patient cells, we established iPS-MLs and iPS-MPs and evaluated their response to various inflammasome activators. Compared with WT counterparts, iPS-MPs derived from Patient 1 produced higher levels of IL-1β and IL-18 in response to *Clostridium difficile* Toxin A (TcdA), a pyrin inflammasome activator, but not to other inflammasome activators such as nigericin and flagellin (Figs. 1 A and S1 B). iPS-MLs exhibited the same pattern, although the levels of IL-1β production were lower than in iPS-MLs, and IL-18 was undetectable (Fig. 1 B). Because IL-6 secretion did not differ between WT and patient-derived clones (Fig. 1, A and B), the elevated production of IL-1β and IL-18 was likely due to an exaggerated response to TcdA rather than a difference in the induction efficacy of iPS-MPs or the genetic background of the cells. The same phenotype was confirmed in cells established from fibroblasts derived from Patient 2 (Fig. S1, C and D). Enhanced formation of apoptosis-associated speck-like protein containing a CARD (ASC) speck in patient-derived iPS-MPs was evident after TcdA stimulation (Fig. 1 C).

Increased IL-1β production from *CDC42*^{R186C} iPS-MLs was inhibited by pyrin inflammasome inhibitors such as colchicine, ABT-751, and CA4P, but not by a nucleotide-binding oligomerization domain-like receptor family pyrin domain-containing 3 (NLRP3) inflammasome inhibitor MCC 950 (Fig. 2 A). IL-1β overproduction and enhanced ASC speck formation in patient-derived clones were suppressed by siRNA-mediated silencing of the *MEFV* gene with no obvious effect on IL-6 production (Fig. 2, B–D). Furthermore, single-base genomic correction of *CDC42*^{R186C} abolished IL-1β overproduction upon LPS and TcdA stimulation, while IL-6 production levels remained unchanged (Fig. 2 E). These findings all confirmed that *CDC42*^{R186C} led to the hyperactivation of pyrin inflammasome.

Aberrant palmitoylation causes trapping of CDC42^{R186C} protein in the Golgi apparatus and induces pyrin activation

Heterozygous mutations of the *CDC42* gene are responsible for Takenouchi–Kosaki syndrome (TKS), which is characterized by developmental delay, facial dysmorphism, and macrothrombocytopenia (Martinelli et al., 2018; Takenouchi et al., 2015; Takenouchi et al., 2016). However, inflammatory manifestations are exceptional in TKS, whereas our patients presented with lethal inflammation soon after birth with no signs of facial dysmorphism or abnormal platelet size. These all suggest that *CDC42*^{R186C} induces different pathophysiology than TKS-associated mutations.

To explore the mechanism of *CDC42*^{R186C}-induced aberrant activation of the pyrin inflammasome, we first compared the guanosine triphosphatase (GTPase) activity of various *CDC42* mutants in human embryonic kidney (HEK) 293T cells by pull-down assay. As previously reported (Martinelli et al., 2018), TKS-associated *CDC42* mutants exhibited diverse derangement in their GTPase activities (Fig. 3 A). However, *CDC42*^{R186C} did not exhibit a significant change in its GTPase activity (Fig. 3 A), consistent with the fact that this mutation is far from the GTP binding site. Instead, the expression level of CDC42^{R186C} protein was elevated, and the electrophoresis mobility was slightly altered (Figs. 3 A and S2 A). This prompted us to check the subcellular distribution of CDC42^{R186C} protein. Consistent with the previous reports (Gernez et al., 2019; Lam et al., 2019), we found that the protein was retained in the Golgi apparatus, a striking feature that is not observed in TKS-associated mutations (Fig. 4).

To determine the molecular basis for the abnormal localization of CDC42^{R186C} protein to the Golgi apparatus, we assessed the binding of each CDC42 mutant to Rho GDP-dissociation inhibitors (GDIs), which modulate the subcellular localization of CDC42. The binding of CDC42^{R186C} protein to Rho-GDI was impaired, as was the binding of some TKS mutants not associated with an inflammatory phenotype, such as CDC42^{R66G} (Fig. 3 B); however, the subcellular distributions of the TKS mutants were comparable with that of the WT CDC42 protein (Fig. 4). *CDC42*^{R66G} iPS-MP clones generated by single-base editing did not produce higher levels of IL-1β in response to LPS and TcdA stimulation (Fig. S2 B). These results suggest that impaired binding of CDC42^{R186C} protein to Rho-GDI is not critical for its localization to the Golgi apparatus or pyrin inflammasome hyperactivation.

Bekhouche et al. (2020) showed that abnormal palmitoylation of CDC42^{R186C} causes its abnormal localization to Golgi apparatus. The *CDC42* transcript is alternatively spliced to produce two isoforms. CDC42 isoform 1 is ubiquitously expressed, and its C-terminal region encodes a -CAAX motif that is geranylgeranylated at Cys^{188}, allowing it to be tethered to cell membranes (Wilson et al., 1998). CDC42 isoform 2 is expressed in the central nervous system, and its C-terminal region is palmitoylated at Cys^{186}, as in the case of the small GTPase H-Ras (Kang et al., 2008). Palmitoylation is a key regulatory step that determines the subcellular distribution of proteins, and the *CDC42*^{R186C} mutation creates a potential palmitoylation site, Cys^{186}, at the C-terminal region of CDC42 isoform 1. By performing acyl–biotin exchange palmitoyl-protein purification from HEK293T cells transfected with CDC42 mutants, we confirmed that CDC42^{R186C}, but not CDC42^{WT} or CDC42^{R66G}, was palmitoylated (Fig. 3 C). We then assessed whether aberrant palmitoylation was responsible for the retention of CDC42^{R186C} protein to the Golgi apparatus in

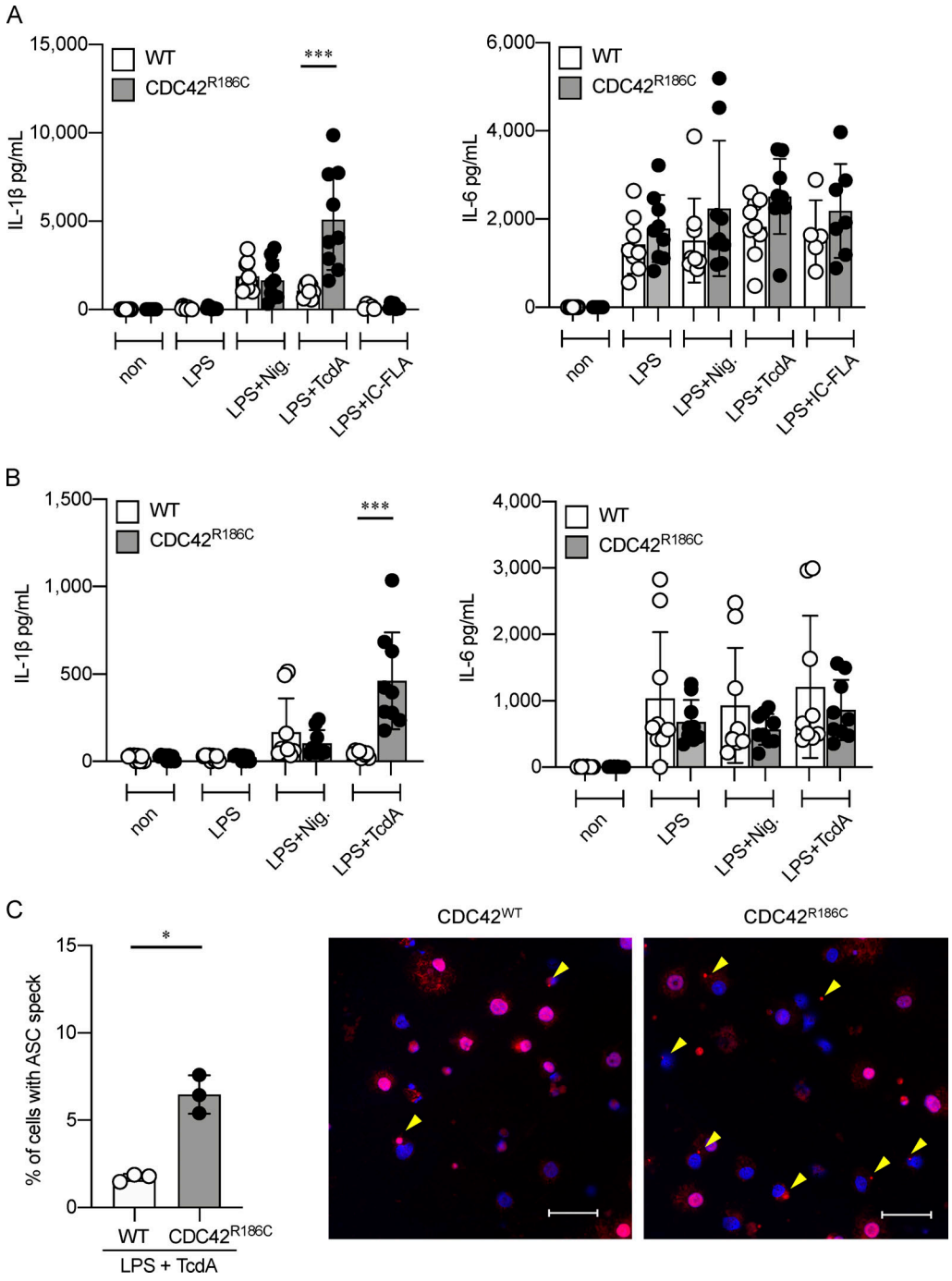

Figure 1. **Response to TcdA stimulation is elevated in iPS-MPs and iPS-MLs derived from a patient carrying CDC42^{R186C}. (A and B)** IL-1β and IL-6 are released in response to various inflammasome stimuli from iPS-derived MPs (A) and MLs (B) established from Patient 1 and healthy controls. The results are from multiple experiments using three independent iPS clones. **(C)** Ratio and representative images of ASC speck formation (arrowheads) in iPS-MPs from Patient 1 and healthy controls after priming with LPS and TcdA. The results are from three experiments with three clones for A and B, and representative results of three independent experiments with three clones are shown in C. *, P < 0.05; ***, P < 0.001; ns, not significant by Mann–Whitney's *U* tests. Scale bars, 50 µm.

HEK293T cells and for IL-1β overproduction by CDC42^{R186C} iPS-MLs by treating cells with the general protein palmitoylation inhibitor 2-bromo-palmitate (2BP). 2BP treatment of HEK293T cells transfected with the *CDC42^{R186C}* mutant decreased its retention in the Golgi apparatus (Fig. 4). Furthermore, 2BP treatment significantly suppressed overproduction of IL-1β from *CDC42^{R186C}* iPS-MLs, but not from iPS-MLs derived from FMF patients carrying *MEFV^{M694I}* (Fig. 3 D). These data indicate that aberrant palmitoylation of CDC42^{R186C} protein caused its retention in the Golgi apparatus and triggered overactivation of the pyrin inflammasome in response to LPS and TcdA stimulation.

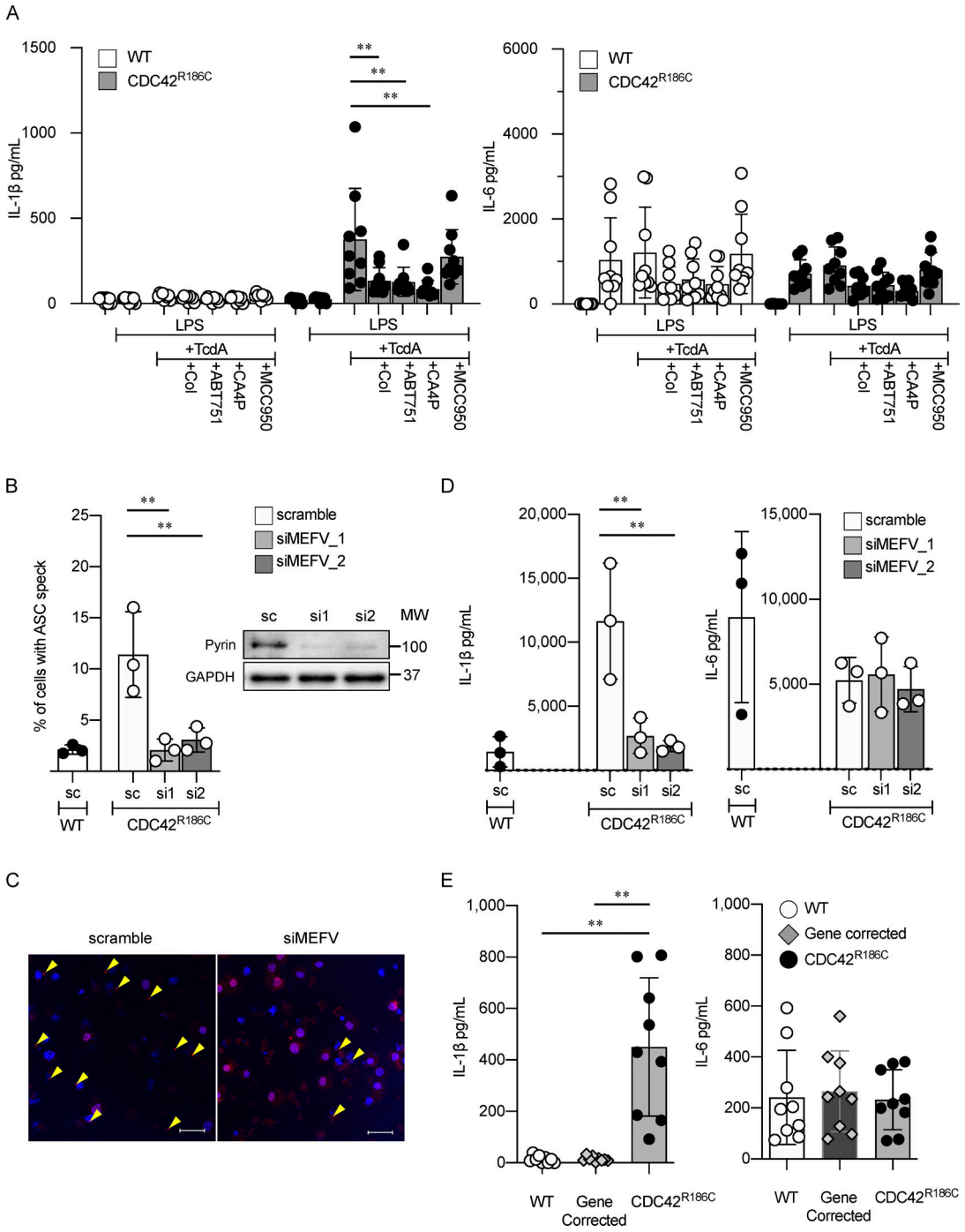

Figure 2. **CDC42^{R186C} induces pyrin inflammasome hyperactivation. (A)** IL-1β and IL-6 release from iPS-MLs derived from Patient 1 and healthy controls stimulated with LPS and TcdA in the presence or absence of pyrin and NLRP3 inhibitors. **(B–D)** Ratio (B) and images (C) of ASC speck formation, and release (D) of IL-1β and IL-6 from Patient 1–derived iPS-MPs in which *MEFV* was knocked down by siRNA. Immunoblot images in B show the effects of siRNAs. **(E)** IL-1β and IL-6 release from Patient 1–derived iPS-MLs, mutation-corrected Patient 1–derived iPS-MLs, and iPS-MLs from healthy controls stimulated with LPS + TcdA. The results in A and E are from three experiments with three clones, and representative results of three independent experiments with three clones are shown for B and D. Statistical significance was determined by Dunnett test in A, B, and D, and by Steel–Dwass test in E. **, $P < 0.01$. Scale bars, 50 µm. Source data are available for this figure: SourceData F2.

CDC42^{R186C} enhances pyrin inflammasome assembly

We then tried to unravel the molecular mechanism of pyrin inflammasome overactivation in *CDC42*^{R186C} cells. Silencing of *CDC42* transcripts suppressed IL-1β production in *CDC42*^{R186C} iPS-MPs after stimulation with TcdA (Fig. S2 C), and also showed a tendency to suppress IL-1β production by WT iPS-MPs. Moreover, silencing of *CDC42* transcripts partially suppressed IL-1β production by these cells after nigericin stimulation (Fig. S2 C), suggesting that CDC42^{WT} is required for full activation of both pyrin and NLRP3 inflammasomes. Together, these

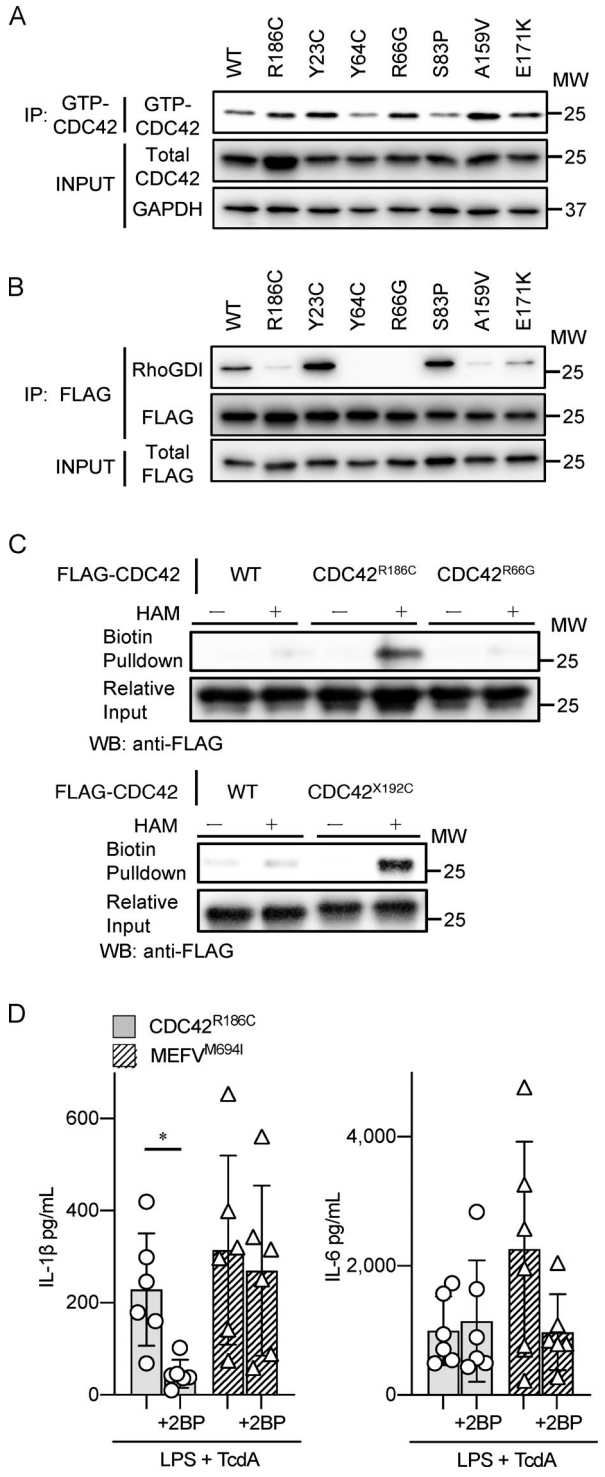

Figure 3. **Palmitoylation of CDC42^{R186C} variant causes IL-1β overproduction. (A)** Immunoblot of GTP-bound CDC42 and total CDC42 in the lysates of HEK293T cells transiently expressing CDC42 variants. **(B)** Interaction of CDC42 variants with Rho-GDI assessed by immunoprecipitation (IPs) of FLAG-tagged CDC42 transiently expressed in HEK293T cells. **(C)** Acyl–biotin exchange assay to evaluate S-palmitoylation levels of FLAG-CDC42 variants expressed in HEK293T cells with or without HAM treatment. **(D)** IL-1β and IL-6 release from iPS-MPs carrying CDC42^{R186C} and MEFV^{M694I} cultured overnight with or without 2BP. Representative results of three independent experiments are shown in A–C, and the results in D are from two experiments with three clones. Statistical significance was determined by unpaired *t* test in D. *, P < 0.05. Source data are available for this figure: SourceData F3.

observations suggest that CDC42^{R186C} is not a simple gain-of-function variant, as it selectively enhanced pyrin, but not NLRP3 inflammasome activation.

To determine how the *CDC42*^{R186C} mutant selectively modulates pyrin inflammasome activation, we compared the characteristics of cells carrying *CDC42*^{R186C} and *MEFV*^{M694I} mutations. Pyrin is phosphorylated at Ser^{208} and Ser^{242} by protein kinase N1 and N2 (PKN1/2), members of the protein kinase C (PKC) family, and at a steady state it is kept inactive by inhibitory 14-3-3 proteins (Gao et al., 2016; Masters et al., 2016; Park et al., 2016; Van Gorp et al., 2016). Recent evidence suggests that the pyrin inflammasome is controlled by two independent mechanisms in healthy donors: pyrin dephosphorylation by inhibition of PKN1/2, followed by inflammasome maturation involving microtubule dynamics. Pyrin molecules harboring FMF-associated *MEFV* mutations, such as *MEFV*^{M694I}, are vulnerable to dephosphorylation stimuli (Magnotti et al., 2019). Overproduction of IL-1β from both *CDC42*^{R186C} and *MEFV*^{M694I} iPS-MLs was inhibited to similar extents by bryostatin (Fig. 5 A), an activator of PKC that phosphorylates pyrin. The inhibitory effect of colchicine, which works predominantly by altering microtubule dynamics, was more potent in *MEFV*^{M694I} iPS-MLs than in *CDC42*^{R186C} iPS-MLs (Fig. 5 B). In addition, stimulation with UCN01, which dephosphorylates pyrin, induced higher levels of IL-1β production in *CDC42*^{R186C} iPS-MLs than in *MEFV*^{M694I} iPS-MLs (Fig. 5 C). Together, these results suggest that CDC42^{R186C} mutant promotes microtubule-dependent assembly of the pyrin inflammasome once pyrin is dephosphorylated.

NF-κB pathway plays a limited role in driving pyrin-dependent autoinflammation, and cytolytic cell function is minimally impaired by *CDC42*^{R186C}

Since increased signaling has been associated with the inflammatory phenotype in patients carrying *CDC42*^{R186C} (Bekhouche et al., 2020), the involvement of the NF-κB pathway was investigated. Analysis of the signaling pathways downstream of LPS priming showed that the phosphorylation of JNK, ERK, p65, and p38 was elevated in *CDC42*^{R186C} cells (Fig. S3 A). However, 2BP treatment had little effect on the phosphorylation of these molecules, with colchicine even enhancing their phosphorylation (Fig. S3 A). Furthermore, pyrin expression did not differ between WT and the mutant cells after LPS priming (Fig. S3 B). These findings indicate that the MAPK and NF-κB pathways do not play a pivotal role in the overactivation of pyrin inflammasomes.

CDC42^{R186C} has been suggested to impair NK cell function and may contribute to the development of HLH (Lam et al., 2019). Analysis of NK cells and cytotoxic T lymphocytes (CTLs) from Patient 1 showed no significant disturbance in the cytolytic activity of NK cells (Fig. S3 C) or in the lysosomal degranulation of both cell types (Fig. S3, D and E), in clear contrast to cells from patients with early-onset familial HLH. These results suggest that CDC42^{R186C} does not severely impair cytolytic pathways to a level that triggers early-onset HLH.

Aberrant subcellular distribution is the common finding of inflammatory CDC42 C-terminal variants

We then asked whether other inflammation-associated CDC42 C-terminal variants have biomolecular characteristics

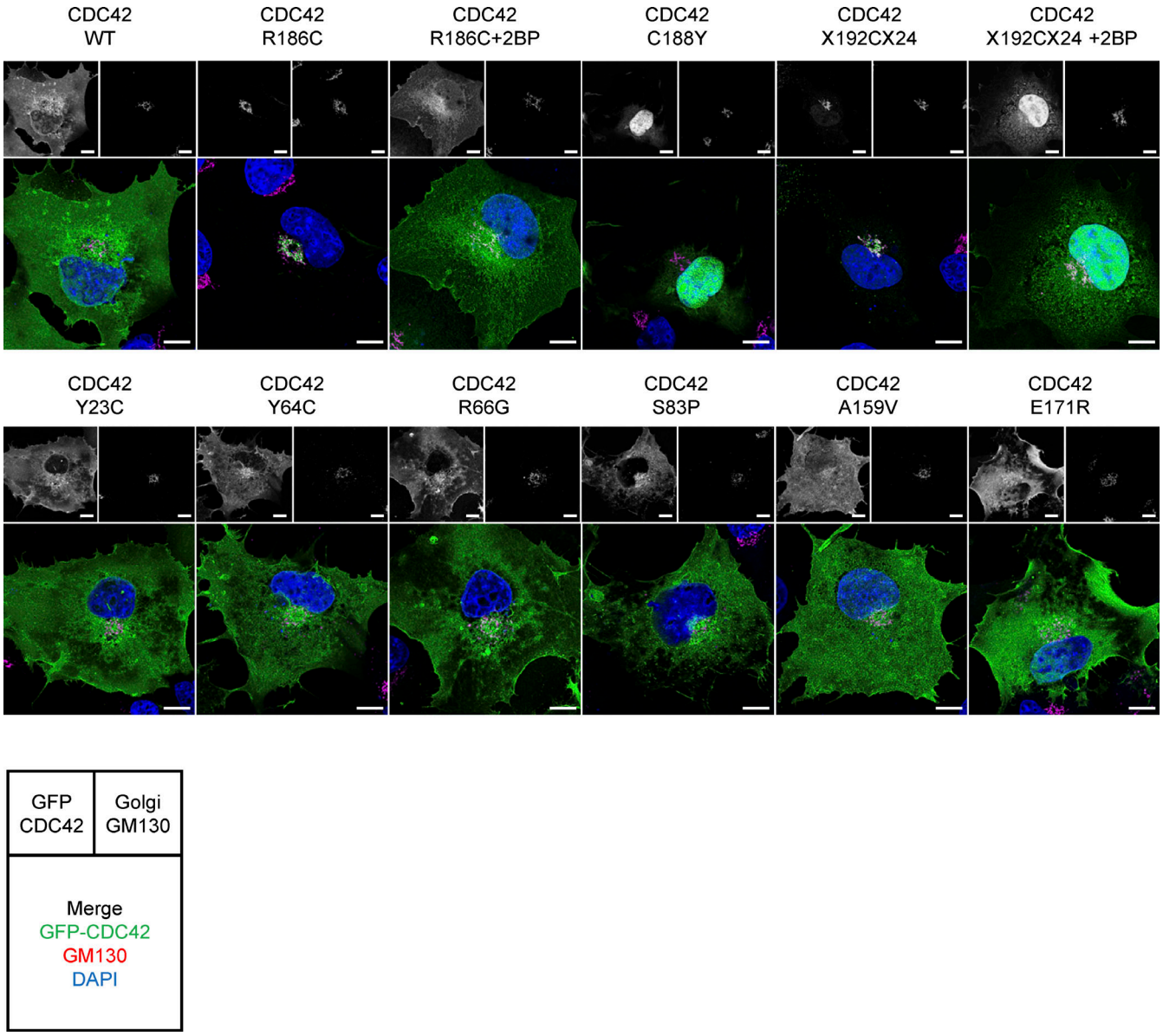

Figure 4. **CDC42^{R186C} variant is palmitoylated and trapped in the Golgi apparatus.** Subcellular distribution of GFP-tagged CDC42 in COS-1 cells with additional images after treatment with 2BP for CDC^{R186C} and CDC42^{*192C*24} variants. Representative results of three independent experiments are shown. Scale bars, 10 µm.

similar to those of CDC42^{R186C}. Indeed, we found that CDC42^{*192C*24} is trapped in the Golgi apparatus, like CDC42^{R186C} (Fig. 4), although less of the former protein accumulated, likely reflecting a difference in the stability of CDC42^{R186C} and CDC42^{*192C*24} mutant proteins (Fig. S2 A). Furthermore, 2BP treatment abolished retention of CDC42^{*192C*24} in the Golgi apparatus (Fig. 4), indicating that CDC42^{*192C*24} is also aberrantly palmitoylated. This finding was supported by the results of acyl–biotin exchange palmitoyl-protein purification assays (Fig. 3 C). Surprisingly, CDC42^{C188Y} was predominantly distributed in the cytoplasm and nucleus, with little retention in the Golgi apparatus (Fig. 4). These results clearly demonstrate that the inflammatory phenotype of patients is associated with aberrant subcellular distribution of CDC42 C-terminal variants.

CDC42^{*192C*24} also induces pyrin inflammasome overactivation

The aberrant subcellular distribution of all the inflammatory CDC42 C-terminal variants prompted us to determine whether CDC42^{C188Y} and CDC42^{*192C*24} induce hyperactivation of the pyrin inflammasome, similar to CDC42^{R186C}. To determine this, we engineered iPSCs to carry CDC42^{WT}, CDC42^{R186C}, CDC42^{C188Y}, and CDC42^{*192C*24} variants in the same genetic background using homologous recombination and evaluated IL-1β production from iPS-MPs. Compared with iPS-MPs carrying CDC42^{WT}, iPS-MPs carrying CDC42^{R186C} and CDC42^{*192C*24}, but not CDC42^{C188Y}, variants produced higher levels of IL-1β specifically in response to LPS and TcdA stimulation. CDC42^{R186C} induced higher levels of IL-1β than CDC42^{*192C*24} (Fig. 6 A),

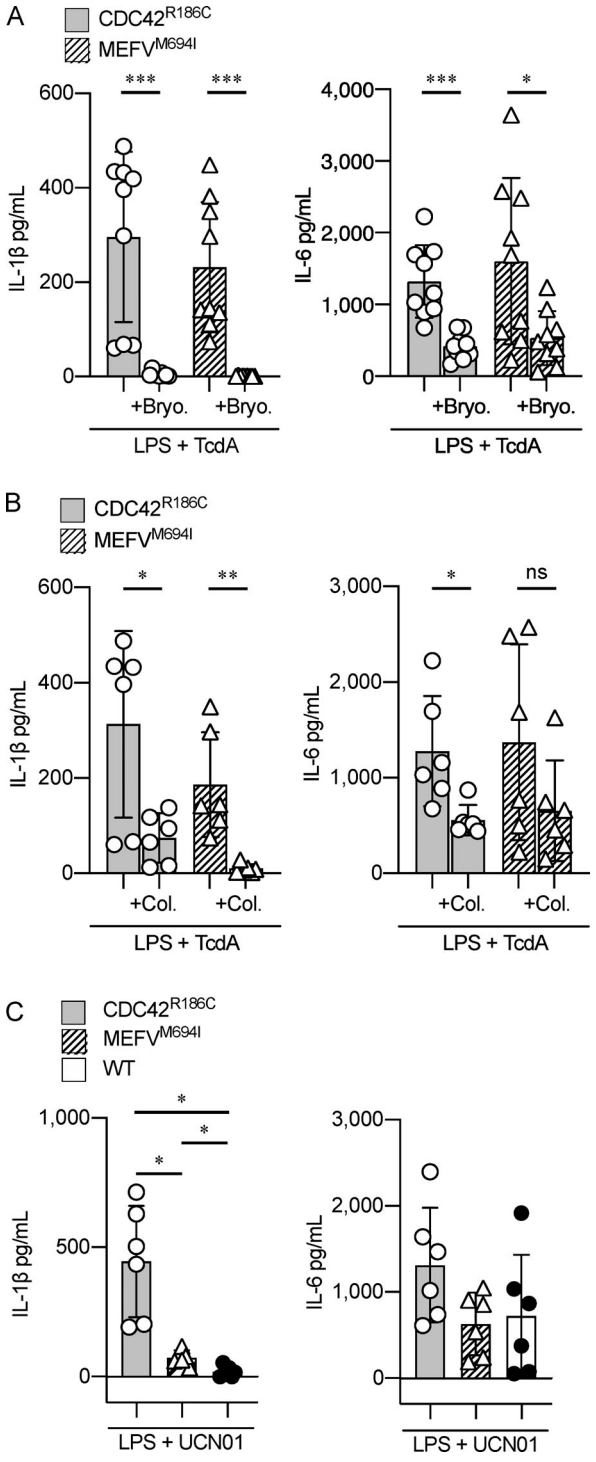

Figure 5. **CDC42^{R186C} promotes pyrin inflammasome assembly. (A and B)** Effect of (A) bryostatin and (B) colchicine on the release of IL-1β and IL-6 from iPS-MLs derived from patients with CDC42^{R186C} and MEFV^{M694I} in response to LPS + TcdA stimulation. **(C)** The release of IL-1β and IL-6 from iPS-MLs derived from healthy donors and patients with CDC42^{R186C} and MEFV^{M994I} after stimulation with UCN01. Results are from two experiments using three independent clones. Statistical significance was determined by unpaired *t* test in A and B, and by Steel–Dwass test in C. *, P < 0.05; **, P < 0.01; ***, P < 0.001; ns, not significant.

paralleling the severity of inflammation reported in the patients and the extent of mutant protein accumulation in the Golgi apparatus. Furthermore, 2BP treatment suppressed IL-1β, but not IL-6 production from CDC42^{R186C} and CDC42^{*192C*24} iPS-MPs (Fig. 6 B), confirming that these two variants induce hyperactivation of the pyrin inflammasome via a similar mechanism.

COP-I–mediated vesicular transport is not impaired by the accumulation of CDC42 C-terminal variants in the Golgi apparatus

Impaired coat protein complex I (COP-I)–mediated vesicular transport triggers autoinflammation (Watkin et al., 2015), and CDC42 regulates COP-I function in a GTPase-dependent manner (Wu et al., 2000). Thus, we decided to determine whether the CDC42^{R186C} and CDC42^{*192C*24} variants impair COP-I–mediated vesicular transport. The expression of these variants did not affect the anterograde membrane traffic of the transmembrane glycoprotein of vesicular stomatitis virus (VSV-G) from the ER to the Golgi (Fig. S4 A) or the retrograde membrane traffic of the stimulator of interferon genes (STING) from the Golgi to the ER (Fig. S4 B), both of which are mediated by the COP-I transport (Mukai et al., 2021; Wu et al., 2000). In addition, the localization of individual COP-I subunits (β-COP, β′-COP, and γ-COP) to the Golgi was not affected by the expression of CDC42 variants (Fig. S4, C–E). These data suggest that the CDC42^{R186C} and CDC42^{*192C*24} variants, unlike those with altered GTPase function, do not impair the COP-I–mediated vesicular transport.

CDC42^{R186C} and CDC42^{*192C*24} variants do not require GTPase activity to induce pyrin hyperactivation

Next, we transfected CDC42 variants with or without WT-pyrin into THP-1 monocytic cells and assessed their effect on the induction of cell death. In the absence of pyrin co-expression, CDC42 variants induced similar levels of THP-1 cell death (Fig. 7 A). The presence of WT-pyrin, CDC42^{R186C}, and CDC42^{*192C*24}, but not CDC42^{C188Y}, increased the frequency of cell death of THP-1 cells to a greater extent than CDC42^{WT} or the non-inflammatory TKS-associated variant CDC42^{R66G} (Fig. 7 A); again, CDC42^{R186C} induced higher levels of cell death than CDC42^{*192C*24}. The increased THP-1 cell death induced by the variants CDC42^{R186C} and CDC42^{*192C*24} was inflammasome-dependent as it was abolished in THP-1 cells lacking caspase-1 (Fig. 7 B). Surprisingly, pyrin-dependent cell death induced by the CDC42^{R186C} and CDC42^{*192C*24} mutants was independent of their GTPase activity because the variants harboring additional T17N mutation, which renders these variants defective in nucleotide-binding (Gibson and Wilson-Delfosse, 2001; Moorman et al., 1999), induced comparable levels of cell death in THP-1 cells (Fig. 7 C). To determine whether pyrin is hyperactivated by the accumulation of a small GTPase other than CDC42 in the Golgi apparatus, THP-1 cells were transfected with a vector expressing a chimeric protein containing Rac1 and the C-terminal tail of CDC42^{R186C} because Rac1^{R187C}, a variant equivalent to CDC42^{R186C}, did not accumulate in the Golgi apparatus (Fig. S5). The chimeric protein accumulated within the Golgi (Fig. S5) but did not increase THP-1 cell death (Fig. 7 D),

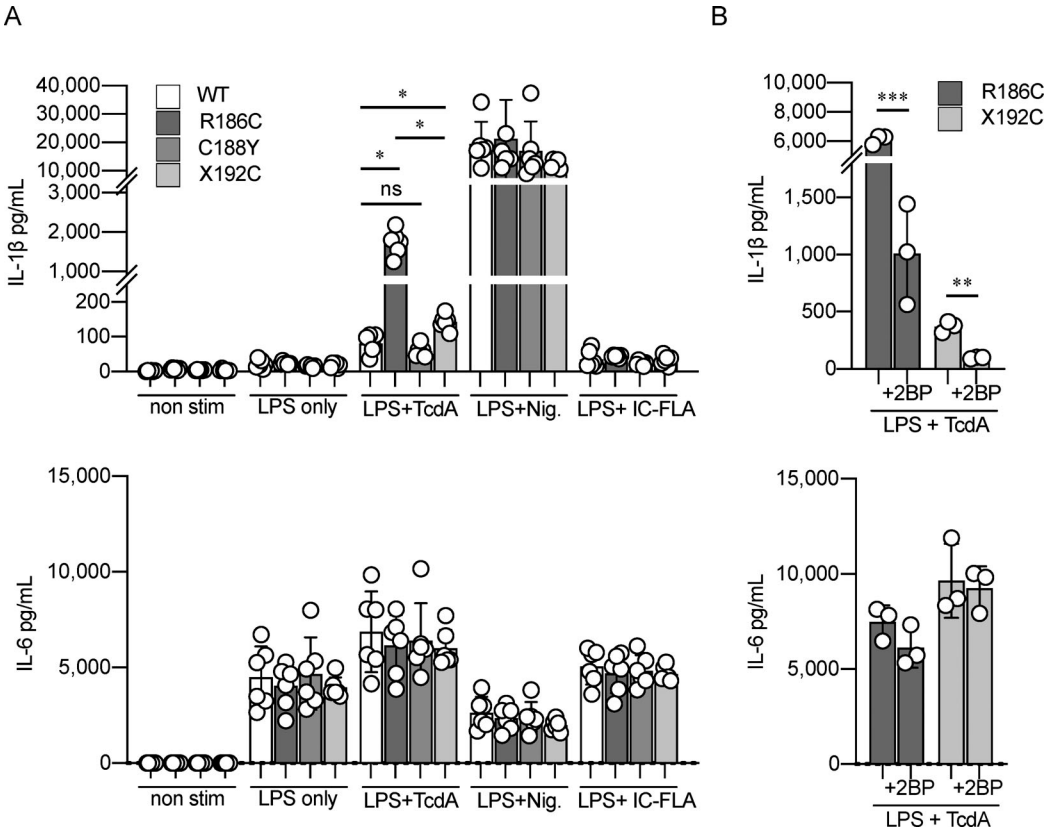

Figure 6. **CDC42^{*192C*24} variant also induces elevated pyrin inflammasome activation. (A)** IL-1β and IL-6 release in response to various inflammasome stimuli from iPS-MPs harboring CDC42^{WT}, CDC42 ^{R186C}, CDC42^{C188Y}, or CDC42^{*192C*24}, all of which were generated from the same iPS clone. **(B)** Effect of 2BP on IL-1β and IL-6 production from iPS-MPs harboring CDC42^{R186C} or CDC42^{*192C*24}. Statistical significance was determined by Steel–Dwass test in A, and by unpaired *t* test in B. The results in A are from two experiments with three clones, and representative results of three independent experiments with three clones are shown for B. *, P < 0.05; **, P < 0.01; ***, P < 0.001; ns, not significant.

suggesting that trapping of CDC42 within the Golgi apparatus specifically triggered pyrin hyperactivation.

Taken together, our results indicate that aberrant subcellular distribution of CDC42 C-terminal variants is associated with inflammatory phenotypes, and that palmitoylation-induced Golgi trapping of CDC42^{R186C} and CDC42^{*192C*24} variants drives pyrin-dependent autoinflammation independently of their GTPase activity.

Discussion

CDC42, a member of the RAS superfamily of low-molecular-weight GTP/GDP-binding proteins, functions as a major node in intracellular signaling including adhesion, migration, polarity, and proliferation (Etienne-Manneville, 2004). CDC42 cycles between a GTP-bound active and a GDP-bound inactive state through regulation by GTPase-activating proteins and guanine nucleotide exchange factors (Heasman and Ridley, 2008). CDC42 has two isoforms. Isoform 1, which is ubiquitously expressed, is tethered to membranes through geranyl-geranylation at a C-terminal Cys^{188} (Wilson et al., 1998). Isoform 2 is expressed in the brain and has alternative C-terminal amino acids, exchanging the prenylation motif for a sequence that is instead palmitoylated (Kang et al., 2008). The intracellular distribution of CDC42 is regulated by these C-terminal modifications and its binding affinity for Rho-GDIs (Garcia-Mata et al., 2011).

In 2015, heterozygous CDC42 mutations were reported to cause TKS, which is characterized by developmental delay, facial dysmorphism, and macrothrombocytopenia (Takenouchi et al., 2015; Takenouchi et al., 2016). Martinelli et al. (2018) showed that GTPase activity and binding affinity for effector molecules vary greatly among TKS-associated CDC42 variants and have proposed phenotype–genotype classification of TKS into three groups; however, inflammatory manifestations are exceptional in TKS. In 2019, a study showed that heterozygous C-terminal variants of CDC42 isoform 1 cause severe and early-onset autoinflammation (Gernez et al., 2019; Lam et al., 2019). Notably in this regard, patients with the CDC42^{R186C} variant present with the most severe inflammation soon after birth but without signs of dysmorphism or macrothrombocytopenia, a phenotype consistent with our two cases (see Case report). However, patients with other C-terminal variants of CDC42 isoform 1 present with both inflammatory and dysmorphic features (Gernez et al., 2019). Recently, inflammation was also reported in a few patients with non–C-terminal CDC42 variants; however, in those individuals, the onset of inflammation was years to decades later, and the features of immunodeficiency were more prominent (Bucciol et al., 2020; Szczawinska-Poplonyk et al.,

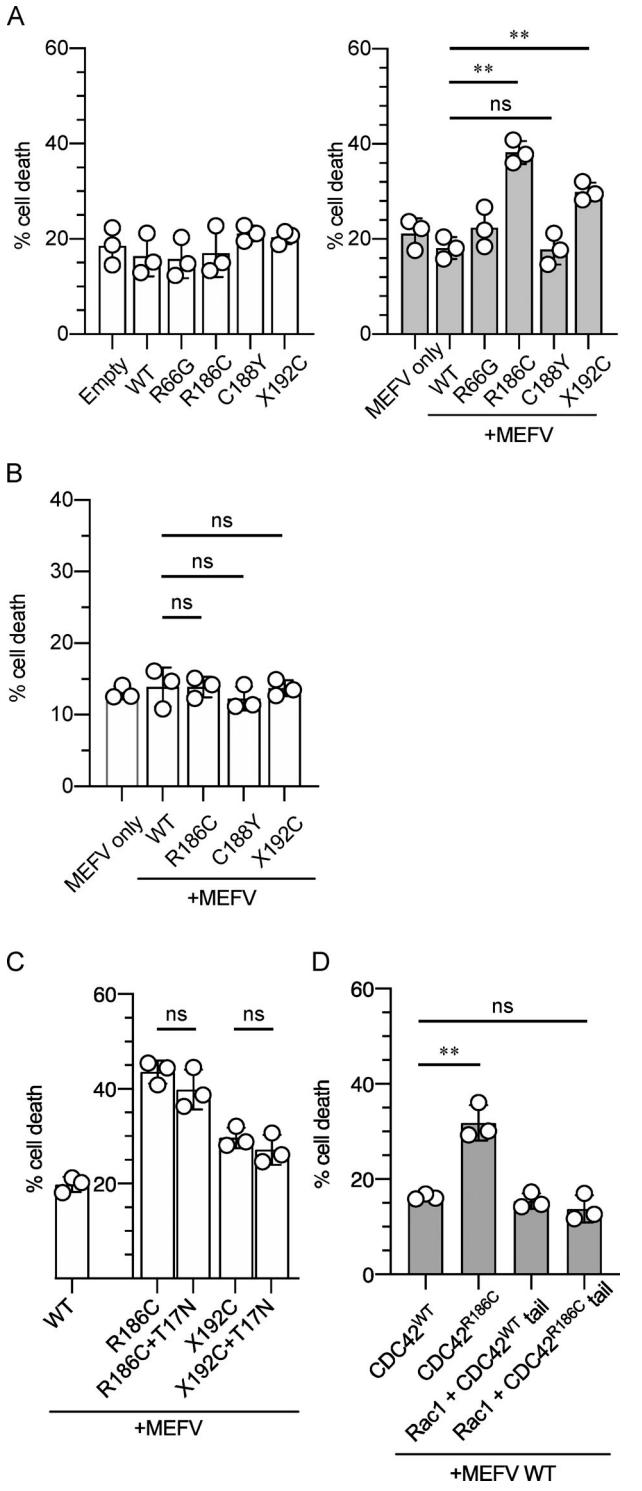

Figure 7. **GTPase activity is dispensable for CDC42^{R186C} and CDC42^{*192C*24} variants to induce pyrin hyperactivation. (A–D)** THP-1 cells (A) or caspase-1 deficient THP-1 cells (B) were nucleofected with WT or CDC42 variants alone or with pyrin, and the proportion of dead cells was evaluated 24 h later. THP-1 cells were nucleofected with (C) pyrin and CDC42 C-terminal variants including those with the additional T17N mutation, or with (D) pyrin and CDC42 C-terminal variants or the chimeric protein containing Rac1 and the C-terminal tail of CDC42. The proportion of dead cells was evaluated 24 h later. Data obtained from three independent experiments are shown. Statistical significance was determined by Dunnett test in A, B, and D, and by unpaired *t* test in C. **, P < 0.01; ns, not significant.

2020). Together, these observations suggest that distinct and complex mechanisms underlie the inflammation and other clinical features caused by CDC42 variants.

In this study, we found that iPS-MLs and -MPs derived from patients carrying the CDC42^{R186C} variant formed higher levels of pyrin inflammasomes. As reported previously, a unique property of the CDC42^{R186C} mutant is its aberrant palmitoylation and localization to the Golgi apparatus (Gernez et al., 2019; Lam et al., 2019). Treatment with a palmitoyl transferase inhibitor released the mutant protein from the Golgi apparatus and normalized the secretion of IL-1β to WT levels. These data clearly illustrate that aberrant palmitoylation of CDC42^{R186C} plays a central role in the retention of the mutant to the Golgi apparatus, as well as in the exaggerated activation of the pyrin inflammasome.

Analysis of the mechanism of pyrin inflammasome overactivation by comparison with cells harboring *MEFV*^{M694I} revealed that the CDC42^{R186C} mutant likely promotes microtubule-dependent assembly of pyrin inflammasomes after pyrin dephosphorylation. Inflammatory pathology driven by the CDC42^{R186C} mutant could not be explained by alteration in GTPase activity or reduced binding affinity for GDIs, as some TKS-causative CDC42 variants that are not associated with inflammatory phenotypes exhibited more severe derangement of these properties. Rather, our results suggest that aberrant subcellular distribution of the variant protein is central to the inflammatory phenotype of the patients with CDC42 C-terminal variants. Due to aberrant palmitoylation, the CDC42^{*192C*24} mutant was also trapped in the Golgi apparatus and induced overactivation of the pyrin inflammasome. Aberrant localization of these variants did not impair vesicular transport mediated by COP-I complex, but the level of IL-1β production paralleled the level of mutant protein accumulation in the Golgi apparatus. Furthermore, pyrin-dependent THP-1 cell death induced by CDC42 C-terminal variants was independent of their GTPase activity. This was further supported by experiments showing that accumulation in the Golgi apparatus of a chimeric protein containing Rac1 and the C-terminal tail of CDC42^{R186C} failed to induce pyrin-dependent THP-1 cell death, suggesting that pyrin-inflammasome overactivation is dependent on the molecular conformation of CDC42 rather than on its GTPase activity. Strong association between the autoinflammatory phenotype and abnormal subcellular localization of the C-terminal CDC42 variants, but not with their altered GTPase activity or binding affinity for GDIs, indicates that ectopic expression of CDC42 molecule drives the assembly of a specific inflammasome through non-physiological pathways.

We acknowledge that the study has several limitations. First, we were unable to reproduce the inflammatory phenotype of cells carrying the CDC42^{C188Y} variant. However, it is possible that the predominantly cytosolic distribution of this mutant is associated with abnormal activation of other inflammasomes. It is also possible that the CDC42^{C188Y} variant may induce inflammation only in specific cell types, such as granulocytes and tissue-resident macrophages, which have different characteristics than iPS-MLs and -MPs. Second, we could not elucidate the molecular mechanism of enhanced pyrin inflammasome assembly induced by Golgi-trapped CDC42 variants. Further

studies are needed to unravel the mechanism that drives the hyperactivation of pyrin and possibly other inflammasomes by C-terminal CDC42 variants.

Our results are consistent with a previous study that reported elevated NF-κB signaling in patient cells (Bekhouche et al., 2020), although it is unlikely that this pathway plays a major role in inducing pyrin inflammasome hyperactivation. However, we believe that this activation of NF-κB signaling contributes to the inflammatory phenotype in patients, especially skin manifestations, as the patient described in that study continued to have skin inflammation even after receiving hematopoietic cell transplantation that resulted in complete donor chimerism (Bekhouche et al., 2020). In regard to another important inflammatory phenotype seen in the patients, it is possible that CDC42^{R186C} impairs NK function and contributes to the development of HLH (Lam et al., 2019). We analyzed NK cells and CTLs derived from Patient 1, but found no significant disturbance in degranulation of both cell types or NK cell cytolytic activity, in clear contrast to the cells from patients with neonatal-onset familial HLH. Because high levels of serum IL-18 cause secondary impairment of NK cell function, which is associated with the development of macrophage activation syndrome (Krei et al., 2021; Weiss et al., 2018), we believe that the HLH phenotype seen in the patients is likely to represent a secondary form. However, because we used cells that were expanded and stimulated with IL-2, which can overcome mild derangement of cytolytic lymphocyte functions (Bryceson et al., 2012; Hori et al., 2017), CDC42^{R186C} itself may mildly impair these functions and contribute to HLH development to some extent.

Of clinical importance, our results suggest that colchicine and other microtubule inhibitors could be used to treat these patients. Because IL-1β blocking therapy was not sufficient to suppress inflammation, and only one patient carrying the CDC42^{R186C} variant has survived for a long period of time without receiving hematopoietic cell transplantation, it would be highly beneficial if these inhibitors were effective in suppressing inflammation.

In conclusion, we have shown that all inflammatory CDC42 C-terminal variants are aberrantly distributed subcellularly, and that palmitoylation-induced trapping of the mutant protein to the Golgi apparatus triggers overactivation of the pyrin inflammasome. Further studies are needed to unravel the complex involvement of CDC42 in the activation of inflammasomes; the resultant knowledge could lead to the development of better management strategies for the patients.

Materials and methods

Study approval

All experiments involving human subjects were conducted in accordance with the principles of the Declaration of Helsinki and were approved by the ethics committee of Kyoto University Hospital (protocol numbers R0091, G0259, and G0457). Written informed consent was obtained from the legal guardians of the patients.

Case report

Patient 1 was a first male child born at term after a noneventful pregnancy to healthy, nonconsanguineous Japanese parents. Starting on the first day of life, he presented with fever, erythema, diarrhea, and hepatosplenomegaly. C-reactive protein (CRP) rose to 182 mg/liter, and pancytopenia (neutrophils 600/μl, hemoglobin 10.3 g/dl, platelets 14.9 × 10^9/liter) was noted. No dysmorphic features were observed, and the patient's platelet size was within the normal range. Extensive microbiological screening returned negative results. Fasting and intravenous administration of high-dose immunoglobulin were partially effective, but their effects were transient, and the patient's condition gradually worsened. Prednisolone (2 mg/kg/d) was started, and the patient's condition stabilized with the recovery of laboratory parameters. CRP became negative, and the count of neutrophils and platelets reached 1,650/μl and 22.5 × 10^9/liter, respectively. However, fever and erythema recurred after gradual tapering of prednisolone. CRP level elevated and pancytopenia worsened, requiring recurrent transfusion of red blood cells and platelets. Bone marrow biopsy revealed hypocellular marrow without remarkable hemophagocytosis. Re-escalation of prednisolone could not suppress inflammation. Etanercept was introduced, but no obvious effect was observed, and the patient died at 4.5 mo of age due to overwhelming inflammation. Patient 2 was a first male child born with body weight of 2,194 g at 36 wk of gestation to healthy nonconsanguineous Japanese parents. On day 6, he presented with fever, erythema multiforme, diarrhea, hepatosplenomegaly, and cholestasis. CRP rose to 48.9 mg/liter, and pancytopenia (neutrophils 860/μl, hemoglobin 12.2 g/dl, platelets 72.0 × 10^9/liter) was noted. The patient's platelet size was within the normal range and he exhibited no dysmorphic features. Extensive screens for infection were all negative and no response was observed to antibacterial and antiviral treatments. Bone marrow examination revealed hypoplastic marrow with scattered foam cells. Dexamethasone therapy was initially effective for the control of symptoms and laboratory parameters. However, the CRP level increased to 380 mg/liter after gradual tapering of dexamethasone. Subsequent steroid therapy with prednisolone and methylprednisolone pulse therapy achieved limited control of intractable inflammation and pancytopenia. Finally, we treated him with plasma exchange therapy. However, the patient died at 2.5 mo of age due to acute respiratory distress syndrome caused by durable and worsening systemic inflammation. Whole-exome sequencing was performed, and a de novo heterozygous c.556C>T variant in CDC42 was identified in both patients.

Generation of iPSCs, iPS-MLs, and iPS-MPs

iPSCs from patients with the *CDC42*^{R186C} variant were generated from peripheral blood mononuclear cells (PBMCs; Patient 1) and fibroblasts (Patient 2) as described previously (Nakagawa et al., 2014). Control iPSC lines were provided by the RIKEN BioResource Center through the National Bio-Resource Project of the Ministry of Education, Culture, Sports, Science, and Technology, Japan. After confirming the quality of the iPSCs, including marker gene expression, the absence of residual vector expression, and pluripotency, iPSC-MLs were established as previously described (Kawasaki et al., 2017). In brief, floating hematopoietic cells that were differentiated into the monocytic

lineage from iPSCs were collected on days 15–18. Cells were transfected with lentiviral constructs encoding BMI1, cMYC, and MDM2 in the CSII-EF-RfA vector kindly provided by Drs. Satoru Senju (Kumamoto University, Kumamoto, Japan) and Hiroyuki Miyoshi (RIKEN BioResource Center, Kyoto, Japan), and cultured in StemPro-34 serum-free medium (Invitrogen) containing Glutamax (Gibco) in the presence of M-CSF (50 ng/ml; R&D Systems) and GM-CSF (50 ng/ml; R&D Systems). For macrophage differentiation, iPS-MLs were cultured in RPMI 1640 medium (Sigma-Aldrich) supplemented with 20% FBS and M-CSF (100 ng/ml) for 6–7 d. Adherent macrophages were detached with Accumax (Innovative Cell Technologies) and collected for subsequent experiments. The morphology and surface marker expression of mutant iPS-MLs and iPS-MPs were comparable with those of the control counterparts.

Single-base editing of CDC42 in iPSCs

Mutation correction (*CDC42*^{R186C} to *CDC42*^{WT}) and mutagenesis (*CDC42*^{WT} to *CDC42*^{R66G}) of the *CDC42* gene in iPSCs were performed by CRSPR-Cas9 adenosine base editing (Gaudelli et al., 2017; Komor et al., 2016). Two adenine base-editor expression vectors with the *EF-1a* promoter and puromycin resistance gene, EF1a-NGG-ABEmax-puroR and EF1a-NG-ABEmax-puroR, were constructed based on pCMV_ABEmax (Koblan et al., 2018), NG-ABEmax (Huang et al., 2019; Addgene plasmid #112095, #124163, gifts from David Liu, Harvard University, Cambridge, MA), and pHL-EF1a-SphcCas9-iP-A (Li et al., 2015; Addgene plasmid #60599, a gift from Akitsu Hotta, Kyoto University, Kyoto, Japan). Single guide (sg) RNA target sites were 5′-ctgcagctcttcttc ggttc-3′ for the correction of *CDC42*^{R186C} (c.556C>T), and 5′-gat gacagattacgaccgctg-3′ for the introduction of *CDC42*^{R66G} (c.A196A>G). sgRNA target oligos were incorporated into sgRNA plasmids: pFYF1320 EGFP Site#1 (Fu et al., 2013), a gift from Keith Joung (Massachusetts General Hospital, Charlestown, MA; Addgene plasmid #47511; http://n2t.net/addgene:47511; RRID: 47511), according to a protocol from David Liu's lab (https://benchling.com/protocols/E64XFSgM/sgrna-plasmid-cloning). sgRNA plasmid (5 µg) and EF1a-NGG/EF1a-NG-ABEmax-puroR (5 µg) were introduced into iPSCs by NEPA21 electroporator (Nepa Gene). 24 h after electroporation, puromycin (1 µg/ml) was added for an additional 24 h. Surviving colonies were picked up, and the genotypes were validated by Sanger sequencing.

Generation of iPSCs carrying CDC42^{WT}, CDC42^{R186C}, CDC42^{C188Y}, and CDC42^{*192C*42} by CRISPR-mediated homologous recombination

iPSC clones carrying *CDC42*^{WT}, *CDC42*^{R186C}, *CDC42*^{C188Y}, and *CDC42*^{*192C*24}, on otherwise identical genetic backgrounds, were generated by CRISPR-mediated homologous recombination, as described previously (Li et al., 2016). In brief, two sgRNA-Cas9 expression vectors (PX458, #43138; Addgene) targeting exon 7 and intron 6 of the *CDC42* gene and targeting vector with a floxed puromycin resistance cassette flanked by 2 kb homology arms were introduced into an iPSC clone derived from a healthy control for homologous recombination. The targeting vectors were constructed with PCR-amplified 3′ and 5′ homology arms, puromycin resistance cassette, and backbone pENTR-DMD-Donor vector (#60605; Addgene) using HiFi DNA Assembly (New England Biolabs). To avoid repeated digestion after successful recombination, synonymous mutations were introduced into PAM sequences of the targeting vector by PCR-based mutagenesis. Each CDC42 variant was also introduced into the corresponding targeting vector by PCR-based mutagenesis. 2 sgRNA-CRISPR/Cas9 vectors (2.5 µg each) and the targeting vector for each mutant (5 µg) were introduced into 1.0 × 10^6 iPSCs using an NEPA 21 electroporator (Nepa Gene). 48–72 h after electroporation, 1 µg/ml puromycin was added. Surviving colonies were picked up and the genotypes were validated by Sanger sequencing. After genotype confirmation, the puromycin resistance cassette was removed by the introduction of the Cre recombinase expression vector.

mRNA silencing

On day 3 of differentiation from iPS-MLs to iPS-MPs, cells were transfected with 60 ng Silencer Select predesigned siRNA (CDC42 siRNA ID: s2765/s55424, MEFV siRNA ID: s502555/s502557; Thermo Fisher Scientific) or Silencer Select Negative Control No. 1 siRNA (Thermo Fisher Scientific) using the Lipofectamine RNAiMAX transfection reagent (Thermo Fisher Scientific).

In vitro stimulation of iPS-MLs and iPS-MPs

iPS-MLs or iPS-MPs were harvested as described above and seeded into 96-well plates at 5 × 10^4 cells per well. When indicated, cells were pretreated with ABT-751 (10 µM; Sigma-Aldrich), CA4P (10 µM; Sigma-Aldrich), MCC950 (10 µM; Sigma-Aldrich), and colchicine (100 ng/ml; Sigma-Aldrich) 30 min before LPS priming or with 2BP (20 µM; Sigma-Aldrich) and bryostatin (0.1 µM; Sigma-Aldrich) 24 h before harvest. For inflammasome activation, cells were primed with LPS (1 µg/ml) for 4 h and treated with UCN-01 (10 µM; Sigma-Aldrich), nigericin (10 µM; Sigma-Aldrich), or purified flagellin from *Salmonella typhimurium* (InvivoGen) in DOTAP liposomes (Roche; IC-FLA; 6 µg DOTAP/1 µg FLA-ST) for an additional 2 h, after which the supernatants were collected. For TcdA stimulation, TcdA (1 µg/ml; List Biological Laboratories) was added after 2 h of LPS priming (1 µg/ml) and the supernatants were collected 4 h later. For AIM2 inflammasome activation, poly (dA; dT)/Lyovec (1 µg/ml; InvivoGen) was added along with LPS priming (1 µg/ml), and the supernatants were collected 4 h later. The IL-1β, IL-18, and IL-6 concentrations were measured using the Bio-Plex Pro Human Cytokine Assay (BioRad).

Immunofluorescence staining and quantification of ASC aggregates

iPS-MPs were stimulated as in the cytokine secretion assay. After 2 h of stimulation with TcdA, the cells were attached to slides with a Cytospin 4 Cytocentrifuge (Thermo Fisher Scientific), fixed in 4% paraformaldehyde, and permeabilized with 0.1% Triton X-100. Cells were incubated with an anti-ASC antibody (Ab) and then with an Alexa Fluor 594–labeled Ab against rabbit IgG. Nuclei were stained with Hoechst. The cells were examined by fluorescence microscopy on a BZ-X710 microscope (Keyence), and the BZ-X Analyzer software (Keyence) was used for quantitative analysis.

Plasmids

The N-terminal FLAG-tagged WT human *CDC42* gene (isoform 1, NP_001782.1) and the puromycin resistance gene separated by a T2A peptide were inserted into the pcDNA5/TO Mammalian Expression Vector by HiFi DNA Assembly to generate a plasmid encoding FLAG-CDC42-t2a-puromycin resistance. An N-terminal-AcGFP–fused CDC42 expression vector was constructed by incorporating PCR-amplified *CDC42* cDNA into the pAcGFP1-C1 Vector (Takara Bio). Each *CDC42* variant was generated by PCR-based mutagenesis using KOD plus (Toyobo). To generate a chimeric protein containing Rac1 and the C-terminal tail of CDC42, plasmids encoding amino acid residues 1 to 162 of WT human Rac1 (NP_008839.2) and amino acid residues 163 to 191 of $CDC42^{WT}$ or $CDC42^{R186C}$ were combined by HiFi DNA Assembly. For co-expression assays with *CDC42* and *MEFV*, a C-terminally GFP-fused *MEFV* gene (isoform 1, NP_000234.1) and *CDC42* separated by T2A peptides were inserted into the pAcGFP1-C1 vector to obtain plasmids encoding hMEFV-pAcGFP1-t2a-CDC42.

Subcellular localization of CDC42, COP-I subunits, and STING

To evaluate the subcellular localization of CDC42 variants and their effect on the distribution of COP-I subunits, COS-1 cells were transfected with AcGFP-CDC42 or AcGFP-T2A-CDC42 using PEI MAX (Polysciences). 24 h after transfection, cells were fixed with 4% paraformaldehyde, permeabilized with 0.1% Triton X-100, and quenched with 50 mM NH_4Cl. After blocking with 3% BSA in PBS, cells were incubated with primary Abs (anti-GM130, 610823; BD Biosciences; anti–β-COP, PA1-061; Thermo Fisher Scientific, anti–β′-COP, A304-523A; Bethyl Laboratories, anti–γ-COP, 12393-I-AP; Proteintech) followed by secondary Abs conjugated to Alexa fluorophore (A-31571 and A-21207; Thermo Fisher Scientific) and then mounted with ProLong Glass Antifade Mountant (P36982; Thermo Fisher Scientific). Nuclei were stained with DAPI (11034-56; Nacalai Tesque).

To evaluate whether STING localization is affected by CDC42 variants, MEFs that stably express EGFP-mouse STING and mScarletI-T2A-CDC42 were established using retroviruses. Plat-E cells were transfected with pMX-IP-EGFP-STING or pMX-IB-mScarletI-T2A-CDC42, and the medium containing the retrovirus was collected. MEFs ($Sting^{-/-}$) were incubated with the medium and then selected with puromycin (2 μg/ml) or blasticidin (5 μg/ml) for several days. Cells were fixed, permeabilized, and stained as described above. Confocal microscopy was performed using LSM880 with Airyscan (Zeiss) with a 63 × 1.4 Plan-Apochromat oil immersion lens or a 100 × 1.46 α Plan-Apochromat oil immersion lens. Images were analyzed and processed with Zeiss ZEN 2.3 SP1 FP3 (black, 64 bit; ver. 14.0.21.201) and Fiji (ver. 2.0.0-rc-69/1.52p).

VSV-G transport assay

COS-1 cells were transfected with VSV-G (tsO45) and mScarletI-T2A-CDC42 using PEI MAX (Polysciences). 6 h later, the medium was replaced with CO_2 independent medium (18045088; Thermo Fisher Scientific) supplemented with 10% FBS, and the cells were incubated for 16 h at 40°C to allow VSV-G to accumulate in the ER. The cells were incubated at 32°C for 30 min to allow for the synchronous release of VSV-G from the ER. The cells were fixed, permeabilized, and stained as described above.

CDC42 transient expression for immunoprecipitation analysis

Plasmids encoding the FLAG-CDC42(WT/mutant)-t2a-puromycin resistance gene or empty vector were transfected into HEK293T cells using Trans-IT 293. 48 h after transfection, puromycin (1 μg/ml) was added for an additional 24 h. The cells were then harvested and assayed for immunoprecipitation analysis.

CDC42 pull-down activation assay

The active, GTP-bound form of CDC42 was pulled down for analysis using the Cdc42 Pull-Down Activation Assay Kit (Cytoskeleton). FLAG-tagged protein pull-down assays were performed using DDDDK-tagged protein purification kit (MBL). Samples were subjected to Western blotting for further analysis.

Acyl–biotin exchange assay for detecting palmitoylated CDC42

The acyl–biotin exchange assay was performed according to a protocol by Junmei Wan (Wan et al., 2007) with minor modifications. HEK293T cells were transfected with the N-terminal FLAG-tagged *CDC42* expression vector using TransIT 293 (Mirus Bio LLC) in 6-well culture plates. After 48 h of transfection, the cells were lysed and subjected to assays. In brief, cell lysates were treated with *N*-ethylmaleimide to block unmodified cysteine-residues on proteins. Palmitoylated cysteines on proteins are cleaved and unmasked by hydroxylamine (HAM) treatment, yielding free cysteines that were previously palmitoylated. Free cysteines were subsequently treated with thiol-reactive HPDP-biotin, and the biotinylated proteins were pulled down with streptavidin beads. Eluted proteins were analyzed by Western blot. Every assay includes a non-HAM treated control to distinguish palmitoylated proteins from nonspecifically biotinylated proteins. A detailed protocol is available upon request.

Western blotting

Protein samples were separated by SDS-PAGE, transferred to polyvinylidene difluoride membrane, and probed with specific primary Abs followed by the HRP-conjugated secondary Abs. Specific bands were visualized by enhanced chemiluminescence using the Clarity Western ECL Substrate (Bio-Rad) and quantified by the ChemiDoc XRS1 System and Image Laboratory software (Bio-Rad). Mouse monoclonal anti-CDC42 (1:1,000; Cytoskeleton), mouse polyclonal GAPDH (1:4,000; FUJIFILM Wako), rabbit polyclonal anti-human pyrin (1:2,000; AdipoGen), mouse monoclonal anti-Rho-GDI (1:500; Santa Cruz Biotechnology), and mouse monoclonal anti-FLAG M2 Ab (1:1,000; Sigma-Aldrich), anti-ERK1/2 (1:1,000; Cell Signaling), anti-p-ERK1/2 (1:1,000; Cell Signaling), anti-p65 (1:1,000; Cell Signaling), anti-p-p65 (1:1,000; Cell Signaling), anti-JNK (1:1,000; Cell Signaling), anti-p-JNK (1:1,000; Cell Signaling), anti-p38 (1:1,000; Cell Signaling), and anti-p-p38 (1:1,000; Cell Signaling) served as primary Abs for Western blotting. HRP-conjugated anti-mouse/rabbit IgG Abs (1:4,000; Jackson ImmunoResearch Laboratories) was used as secondary Abs.

Nucleofection and flow cytometry

THP-1 nucleofection and cell death assays were performed as described previously (Fujisawa et al., 2007; Honda et al., 2021) with some modifications. THP-1 cells (1×10^6) were transfected with 500 ng plasmid encoding pAcGFP-fused CDC42 variants or *hMEFV*-pAcGFP1-t2a-*CDC42* using 4D-Nucleofector and the SG Cell Line 4D-Nucleofector X Kit (Lonza). Immediately after nucleofection, 10 ng/ml phorbol 12-myristate 13-acetate (FUJIFILM Wako) was added and the cells were cultured overnight. The next day, the cells were stained with LIVE/DEAD Fixable Violet Dead Cell Stain Kit (Thermo Fisher Scientific) as indicated. Cells were analyzed using a FACSVerse flow cytometer (Becton and Dickinson Bioscience [BD]) and FlowJo software (BD). Cell death was calculated as the percentage of the size-gated cells that were BV421-high.

NK cell cytolytic assay

PBMCs were stimulated and expanded in NK MACS Medium (Miltenyi Biotec) for >3 wk. These cells were co-cultured for 6 h with K562 cells in 96-well microtiter plates as targets, and the cytolytic activity was determined in an LDH release assay (Non-Radioactive Cytotoxicity Assay; CytoTox 96 Assay; Promega). Background spontaneous and maximal LDH release were determined by culturing target cells in medium alone or medium containing Triton X-100.

Degranulation assays

To quantify lysosome exocytosis by NK cells, 2×10^5 PBMCs stimulated for 48 h with human recombinant interleukin-2 (rIL-2, 50 μ/ml) were cultured with or without 2×10^5 K562 cells and incubated for 2 h. Lysosomal degranulation of cytolytic T cells (CTLs) was evaluated using alloantigen-specific $CD8^+$ CTL lines as described previously (Nagai et al., 2010; Shibata et al., 2018). Briefly, PBMCs obtained from patients and healthy individuals were co-cultured with a mitomycin C (MMC)–treated B-lymphoblastoid cell line (KI-LCL) established from an HLA-mismatched individual. 6 d later, $CD8^+$ T lymphocytes were isolated using immunomagnetic beads (MACS beads; Miltenyi Biotec). The cells were cultured in RPMI 1640 medium supplemented with 10% human serum and 10 IU/ml human rIL-2 and stimulated weekly with MMC-treated KI-LCL cells for >3 wk. These lymphocytes (2×10^5 in 96-well round-bottom plates) were mixed with an equal number of P815 cells in the presence of 0.5 μg/ml anti-CD3 mAb (OKT3) for 2 h. Cells were resuspended in PBS supplemented with 2% FCS and 2 mM EDTA; stained with anti-CD3, anti-CD8, anti-CD56, and anti-CD107a Abs; and analyzed by flow cytometry.

Statistical analysis

Results in independent cell lines were compared by Mann–Whitney's *U* tests for two groups or by Steel–Dwass tests for multiple comparisons. The effect of procedure(s) on single-cell lines were compared by unpaired *t*-tests for two groups or by Dunnett tests for multiple comparisons. All statistical analyses were performed using Statcel software ver. 4 (OMS Publishing), with $P < 0.05$ considered statistically significant.

Online supplemental material

Fig. S1 shows the increased production of IL-1β and IL-18 in patients with $CDC42^{R186C}$. Fig. S2 shows the immunoblot analysis of CDC42 C-terminal variants, cytokine production from iPS-MLs carrying $CDC42^{R66G}$, and the effect of CDC42 silencing on cytokine production from $CDC42^{WT}$ and $CDC42^{R186C}$ iPS-MLs. Fig. S3 shows the results of NF-κB signaling analyses of iPS-MLs and cytolytic and degranulation activity of NK cells and CTLs from Patient 1. Fig. S4 shows that $CDC42^{R186C}$ and $CDC42^{*192C*24}$ variants do not affect the transport and the localization of COP-I. Fig. S5 shows that the addition of the C-terminal sequence of $CDC42^{R186C}$ to Rac1 alters its localization to the Golgi.

Acknowledgments

The authors are grateful to the patients and their families.

This work was supported by JSPS KAKENHI (grant numbers 21K07795, 20H03202, and 19H00974), AMED (grant numbers JP20ek0109387, JP21bm0104001, JP21bm0804005, JP19bm0804001, and JP20gm5910025), the "Research on Measures for Intractable Diseases" project from the Japanese Ministry of Health, Labour and Welfare, and by the Mochida Memorial Foundation for Medical and Pharmaceutical Research.

Author contributions: R. Nishikomori, T. Taguchi, Y. Sasahara, and T. Yasumi designed the research; M. Nishitani-Isa performed genetic manipulation of iPSCs, cell culture and stimulation assays, Western blotting, and pull down assays; K. Mukai performed immunocytochemical analyses; O. Ohara performed genetic analysis; Y. Kawasaki., M. Osawa, and M. Saito generated iPSCs and iPS-MLs; Y. Honda, H. Nihira, T. Tanaka, H. Shibata, K. Kodama, T. Uchida assisted in the research; M. Nishitani-Isa, Y. Honda, H. Nihira, T. Tanaka, H. Shibata, K. Izawa, Y. Katata, S. Onodera., T. Watanabe, R. Nishikomori, and T. Yasumi attended to the patients; M. Nishitani-Isa, K. Mukai, Y. Honda, T. Tanaka, E. Hiejima, K. Izawa, S. Kure, J. Takita, R. Nishikomori, T. Taguchi, Y. Sasahara, and T. Yasumi analyzed the data and discussed the results; M. Nishitani-Isa, K. Mukai, Y. Honda, and T. Yasumi wrote the paper.

Disclosures: The authors declare no competing interests exist.

Submitted: 6 September 2021
Revised: 28 February 2022
Accepted: 31 March 2022

References

Bekhouche, B., A. Tourville, Y. Ravichandran, R. Tacine, L. Abrami, M. Dussiot, A. Khau-Dancasius, O. Boccara, M. Khirat, M. Mangeney, et al. 2020. A toxic palmitoylation of Cdc42 enhances NF-κB signaling and drives a severe autoinflammatory syndrome. *J. Allergy Clin. Immunol.* 146:1201–1204.e8. https://doi.org/10.1016/j.jaci.2020.03.020

Bryceson, Y.T., D. Pende, A. Maul-Pavicic, K.C. Gilmour, H. Ufheil, T. Vraetz, S.C. Chiang, S. Marcenaro, R. Meazza, I. Bondzio, et al. 2012. A prospective evaluation of degranulation assays in the rapid diagnosis of familial hemophagocytic syndromes. *Blood.* 119:2754–2763. https://doi.org/10.1182/blood-2011-08-374199

Bucciol, G., B. Pillay, J. Casas-Martin, S. Delafontaine, M. Proesmans, N. Lorent, J. Coolen, T. Tousseyn, X. Bossuyt, C.S. Ma, et al. 2020. Systemic inflammation and myelofibrosis in a patient with takenouchi-kosaki

syndrome due to CDC42 Tyr64Cys mutation. *J. Clin. Immunol.* 40: 567–570. https://doi.org/10.1007/s10875-020-00742-5

Chae, J.J., Y.H. Cho, G.S. Lee, J. Cheng, P.P. Liu, L. Feigenbaum, S.I. Katz, and D.L. Kastner. 2011. Gain-of-function Pyrin mutations induce NLRP3 protein-independent interleukin-1β activation and severe autoinflammation in mice. *Immunity*. 34:755–768. https://doi.org/10.1016/j.immuni.2011.02.020

Etienne-Manneville, S. 2004. Cdc42-the centre of polarity. *J. Cell Sci.* 117: 1291–1300. https://doi.org/10.1242/jcs.01115

Fu, Y., J.A. Foden, C. Khayter, M.L. Maeder, D. Reyon, J.K. Joung, and J.D. Sander. 2013. High-frequency off-target mutagenesis induced by CRISPR-Cas nucleases in human cells. *Nat. Biotechnol.* 31:822–826. https://doi.org/10.1038/nbt.2623

Fujisawa, A., N. Kambe, M. Saito, R. Nishikomori, H. Tanizaki, N. Kanazawa, S. Adachi, T. Heike, J. Sagara, T. Suda, et al. 2007. Disease-associated mutations in CIAS1 induce cathepsin B-dependent rapid cell death of human THP-1 monocytic cells. *Blood*. 109:2903–2911. https://doi.org/10.1182/blood-2006-07-033597

Gao, W., J. Yang, W. Liu, Y. Wang, and F. Shao. 2016. Site-specific phosphorylation and microtubule dynamics control Pyrin inflammasome activation. *Proc. Natl. Acad. Sci. USA*. 113:E4857–E4866. https://doi.org/10.1073/pnas.1601700113

Garcia-Mata, R., E. Boulter, and K. Burridge. 2011. The "invisible hand": Regulation of RHO GTPases by RHOGDIs. *Nat. Rev. Mol. Cell Biol.* 12: 493–504. https://doi.org/10.1038/nrm3153

Gaudelli, N.M., A.C. Komor, H.A. Rees, M.S. Packer, A.H. Badran, D.I. Bryson, and D.R. Liu. 2017. Programmable base editing of A•T to G•C in genomic DNA without DNA cleavage. *Nature*. 551:464–471. https://doi.org/10.1038/nature24644

Gernez, Y., A.A. De Jesus, H. Alsaleem, C. Macaubas, A. Roy, D. Lovell, K.A. Jagadeesh, S. Alehashemi, L. Erdman, M. Grimley, et al. 2019. Severe autoinflammation in 4 patients with C-terminal variants in cell division control protein 42 homolog (CDC42) successfully treated with IL-1β inhibition. *J. Allergy Clin. Immunol.* 144:1122–1125.e6. https://doi.org/10.1016/j.jaci.2019.06.017

Gibson, R.M., and A.L. Wilson-Delfosse. 2001. RhoGDI-binding-defective mutant of Cdc42Hs targets to membranes and activates filopodia formation but does not cycle with the cytosol of mammalian cells. *Biochem. J.* 359:285–294. https://doi.org/10.1042/0264-6021:3590285

Heasman, S.J., and A.J. Ridley. 2008. Mammalian Rho GTPases: New insights into their functions from in vivo studies. *Nat. Rev. Mol. Cell Biol.* 9: 690–701. https://doi.org/10.1038/nrm2476

Honda, Y., Y. Maeda, K. Izawa, T. Shiba, T. Tanaka, H. Nakaseko, K. Nishimura, H. Mukoyama, M. Isa-Nishitani, T. Miyamoto, et al. 2021. Rapid flow cytometry-based assay for the functional classification of MEFV variants. *J. Clin. Immunol.* 41:1187–1197. https://doi.org/10.1007/s10875-021-01021-7

Hori, M., T. Yasumi, S. Shimodera, H. Shibata, E. Hiejima, H. Oda, K. Izawa, T. Kawai, M. Ishimura, N. Nakano, et al. 2017. A CD57^{+} CTL degranulation assay effectively identifies familial hemophagocytic lymphohistiocytosis type 3 patients. *J. Clin. Immunol.* 37:92–99. https://doi.org/10.1007/s10875-016-0357-3

Huang, T.P., K.T. Zhao, S.M. Miller, N.M. Gaudelli, B.L. Oakes, C. Fellmann, D.F. Savage, and D.R. Liu. 2019. Circularly permuted and PAM-modified Cas9 variants broaden the targeting scope of base editors. *Nat. Biotechnol.* 37:626–631. https://doi.org/10.1038/s41587-019-0134-y

Kang, R., J. Wan, P. Arstikaitis, H. Takahashi, K. Huang, A.O. Bailey, J.X. Thompson, A.F. Roth, R.C. Drisdel, R. Mastro, et al. 2008. Neural palmitoyl-proteomics reveals dynamic synaptic palmitoylation. *Nature*. 456:904–909. https://doi.org/10.1038/nature07605

Kawasaki, Y., H. Oda, J. Ito, A. Niwa, T. Tanaka, A. Hijikata, R. Seki, A. Nagahashi, M. Osawa, I. Asaka, et al. 2017. Identification of a high-frequency somatic NLRC4 mutation as a cause of autoinflammation by pluripotent cell-based phenotype dissection. *Arthritis Rheumatol.* 69: 447–459. https://doi.org/10.1002/art.39960

Koblan, L.W., J.L. Doman, C. Wilson, J.M. Levy, T. Tay, G.A. Newby, J.P. Maianti, A. Raguram, and D.R. Liu. 2018. Improving cytidine and adenine base editors by expression optimization and ancestral reconstruction. *Nat. Biotechnol.* 36:843–846. https://doi.org/10.1038/nbt.4172

Komor, A.C., Y.B. Kim, M.S. Packer, J.A. Zuris, and D.R. Liu. 2016. Programmable editing of a target base in genomic DNA without double-stranded DNA cleavage. *Nature*. 533:420–424. https://doi.org/10.1038/nature17946

Krei, J.M., H.J. Møller, and J.B. Larsen. 2021. The role of interleukin-18 in the diagnosis and monitoring of hemophagocytic lymphohistiocytosis/macrophage activation syndrome: A systematic review. *Clin. Exp. Immunol.* 203:174–182. https://doi.org/10.1111/cei.13543

Lam, M.T., S. Coppola, O.H.F. Krumbach, G. Prencipe, A. Insalaco, C. Cifaldi, I. Brigida, E. Zara, S. Scala, S. Di Cesare, et al. 2019. A novel disorder involving dyshematopoiesis, inflammation, and HLH due to aberrant CDC42 function. *J. Exp. Med.* 216:2778–2799. https://doi.org/10.1084/jem.20190147

Li, H.L., N. Fujimoto, N. Sasakawa, S. Shirai, T. Ohkame, T. Sakuma, M. Tanaka, N. Amano, A. Watanabe, H. Sakurai, et al. 2015. Precise correction of the dystrophin gene in duchenne muscular dystrophy patient induced pluripotent stem cells by TALEN and CRISPR-Cas9. *Stem Cell Rep.* 4:143–154. https://doi.org/10.1016/j.stemcr.2014.10.013

Li, H.L., P. Gee, K. Ishida, and A. Hotta. 2016. Efficient genomic correction methods in human iPS cells using CRISPR-Cas9 system. *Methods*. 101: 27–35. https://doi.org/10.1016/j.ymeth.2015.10.015

Magnotti, F., L. Lefeuvre, S. Benezech, T. Malsot, L. Waeckel, A. Martin, S. Kerever, D. Chirita, M. Desjonqueres, A. Duquesne, et al. 2019. Pyrin dephosphorylation is sufficient to trigger inflammasome activation in familial Mediterranean fever patients. *EMBO Mol Med.* 11:e10547. https://doi.org/10.15252/emmm.201910547

Manthiram, K., Q. Zhou, I. Aksentijevich, and D.L. Kastner. 2017. The monogenic autoinflammatory diseases define new pathways in human innate immunity and inflammation. *Nat. Immunol.* 18:832–842. https://doi.org/10.1038/ni.3777

Martinelli, S., O.H.F. Krumbach, F. Pantaleoni, S. Coppola, E. Amin, L. Pannone, K. Nouri, L. Farina, R. Dvorsky, F. Lepri, et al. 2018. Functional dysregulation of CDC42 causes diverse developmental phenotypes. *Am. J. Hum. Genet.* 102:309–320. https://doi.org/10.1016/j.ajhg.2017.12.015

Masters, S.L., V. Lagou, I. Jéru, P.J. Baker, L. Van Eyck, D.A. Parry, D. Lawless, D. De Nardo, J.E. Garcia-Perez, L.F. Dagley, et al. 2016. Familial autoinflammation with neutrophilic dermatosis reveals a regulatory mechanism of pyrin activation. *Sci. Transl. Med.* 8:332ra45. https://doi.org/10.1126/scitranslmed.aaf1471

McDermott, M.F., I. Aksentijevich, J. Galon, E.M. McDermott, B.W. Ogunkolade, M. Centola, E. Mansfield, M. Gadina, L. Karenko, T. Pettersson, et al. 1999. Germline mutations in the extracellular domains of the 55 kDa TNF receptor, TNFR1, define a family of dominantly inherited autoinflammatory syndromes. *Cell*. 97:133–144. https://doi.org/10.1016/s0092-8674(00)80721-7

Moorman, J.P., D. Luu, J. Wickham, D.A. Bobak, and C.S. Hahn. 1999. A balance of signaling by Rho family small GTPases RhoA, Rac1 and Cdc42 coordinates cytoskeletal morphology but not cell survival. *Oncogene*. 18: 47–57. https://doi.org/10.1038/sj.onc.1202262

Mukai, K., E. Ogawa, R. Uematsu, Y. Kuchitsu, F. Kiku, T. Uemura, S. Waguri, T. Suzuki, N. Dohmae, H. Arai, et al. 2021. Homeostatic regulation of STING by retrograde membrane traffic to the ER. *Nat. Commun.* 12:61. https://doi.org/10.1038/s41467-020-20234-9

Nagai, K., K. Yamamoto, H. Fujiwara, J. An, T. Ochi, K. Suemori, T. Yasumi, H. Tauchi, K. Koh, M. Sato, et al. 2010. Subtypes of familial hemophagocytic lymphohistiocytosis in Japan based on genetic and functional analyses of cytotoxic T lymphocytes. *PLoS One*. 5:e14173. https://doi.org/10.1371/journal.pone.0014173

Nakagawa, M., Y. Taniguchi, S. Senda, N. Takizawa, T. Ichisaka, K. Asano, A. Morizane, D. Doi, J. Takahashi, M. Nishizawa, et al. 2014. A novel efficient feeder-free culture system for the derivation of human induced pluripotent stem cells. *Sci. Rep.* 4:3594. https://doi.org/10.1038/srep03594

Nigrovic, P.A., P.Y. Lee, and H.M. Hoffman. 2020. Monogenic autoinflammatory disorders: Conceptual overview, phenotype, and clinical approach. *J. Allergy Clin. Immunol.* 146:925–937. https://doi.org/10.1016/j.jaci.2020.08.017

Park, Y.H., G. Wood, D.L. Kastner, and J.J. Chae. 2016. Pyrin inflammasome activation and RhoA signaling in the autoinflammatory diseases FMF and HIDS. *Nat. Immunol.* 17:914–921. https://doi.org/10.1038/ni.3457

Saito, M.K. 2021. Elucidation of the pathogenesis of autoinflammatory diseases using iPS cells. *Children*. 8:94. https://doi.org/10.3390/children8020094

Shibata, H., T. Yasumi, S. Shimodera, E. Hiejima, K. Izawa, T. Kawai, R. Shirakawa, T. Wada, R. Nishikomori, H. Horiuchi, et al. 2018. Human CTL-based functional analysis shows the reliability of a munc13-4 protein expression assay for FHL3 diagnosis. *Blood*. 131:2016–2025. https://doi.org/10.1182/blood-2017-10-812503

Szczawinska-Poplonyk, A., R. Ploski, E. Bernatowska, and M. Pac. 2020. A novel *CDC42* mutation in an 11-year old child manifesting as syndromic immunodeficiency, autoinflammation, hemophagocytic lymphohistiocytosis,

and malignancy: A case report. *Front. Immunol.* 11:318. https://doi.org/10.3389/fimmu.2020.00318

Takenouchi, T., R. Kosaki, T. Niizuma, K. Hata, and K. Kosaki. 2015. Macrothrombocytopenia and developmental delay with a de novo CDC42 mutation: Yet another locus for thrombocytopenia and developmental delay. *Am. J. Med. Genet. A.* 167A:2822–2825. https://doi.org/10.1002/ajmg.a.37275

Takenouchi, T., N. Okamoto, S. Ida, T. Uehara, and K. Kosaki. 2016. Further evidence of a mutation in CDC42 as a cause of a recognizable syndromic form of thrombocytopenia. *Am. J. Med. Genet. A.* 170A:852–855. https://doi.org/10.1002/ajmg.a.37526

Van Gorp, H., P.H.V. Saavedra, N.M. De Vasconcelos, N. Van Opdenbosch, L. Vande Walle, M. Matusiak, G. Prencipe, A. Insalaco, F. Van Hauwermeiren, D. Demon, et al. 2016. Familial Mediterranean fever mutations lift the obligatory requirement for microtubules in Pyrin inflammasome activation. *Proc. Natl. Acad. Sci. USA.* 113:14384–14389. https://doi.org/10.1073/pnas.1613156113

Wan, J., A.F. Roth, A.O. Bailey, and N.G. Davis. 2007. Palmitoylated proteins: Purification and identification. *Nat. Protoc.* 2:1573–1584. https://doi.org/10.1038/nprot.2007.225

Watkin, L.B., B. Jessen, W. Wiszniewski, T.J. Vece, M. Jan, Y. Sha, M. Thamsen, R.L.P. Santos-Cortez, K. Lee, T. Gambin, et al. 2015. COPA mutations impair ER-Golgi transport and cause hereditary autoimmune-mediated lung disease and arthritis. *Nat. Genet.* 47:654–660. https://doi.org/10.1038/ng.3279

Weiss, E.S., C. Girard-Guyonvarc'h, D. Holzinger, A.A. de Jesus, Z. Tariq, J. Picarsic, E.J. Schiffrin, D. Foell, A.A. Grom, S. Ammann, et al. 2018. Interleukin-18 diagnostically distinguishes and pathogenically promotes human and murine macrophage activation syndrome. *Blood.* 131:1442–1455. https://doi.org/10.1182/blood-2017-12-820852

Wilson, A.L., R.A. Erdman, F. Castellano, and W.A. Maltese. 1998. Prenylation of Rab8 GTPase by type I and type II geranylgeranyl transferases. *Biochem. J.* 333:497–504. https://doi.org/10.1042/bj3330497

Wu, W.J., J.W. Erickson, R. Lin, and R.A. Cerione. 2000. The gamma-subunit of the coatomer complex binds Cdc42 to mediate transformation. *Nature.* 405:800–804. https://doi.org/10.1038/35015585

JEM

Supplemental material

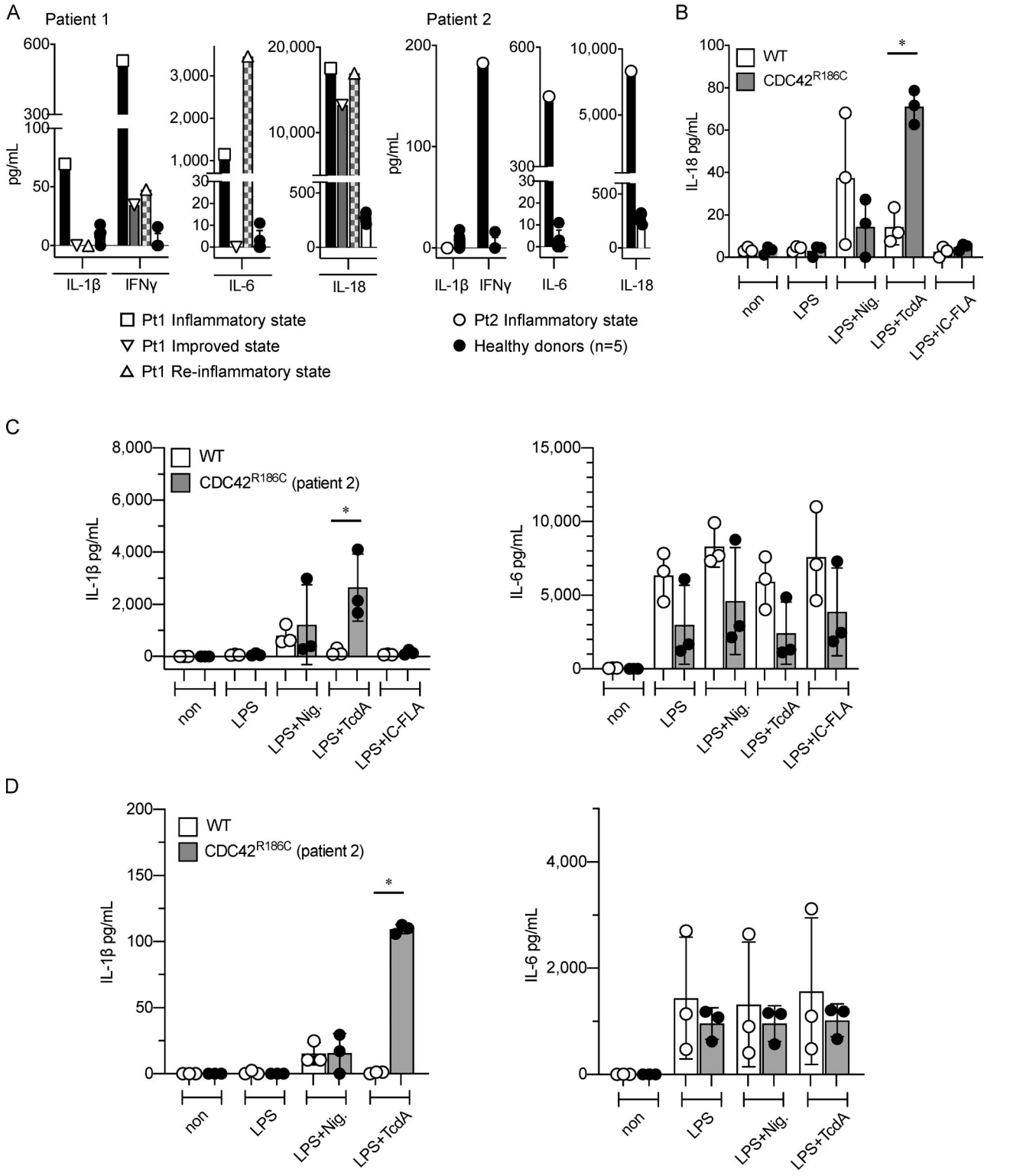

Figure S1. **Increased production of IL-1β and IL-18 in patients carrying *CDC42*^{R186C}. (A)** Levels of IL-1β, IL-6, IL-18, and IFNγ in sera of Patients 1 and 2. **(B)** IL-18 release in response to various inflammasome stimuli from iPS-derived MPs established from Patient 1 and healthy controls. **(C and D)** IL-1β and IL-6 release in response to various inflammasome stimuli from iPS-derived MPs (C) and MLs (D) established from Patient 2 and healthy controls. Data are representative of two independent experiments using three independent clones. Statistical significance was determined by Mann–Whitney's *U* test. *, P < 0.05.

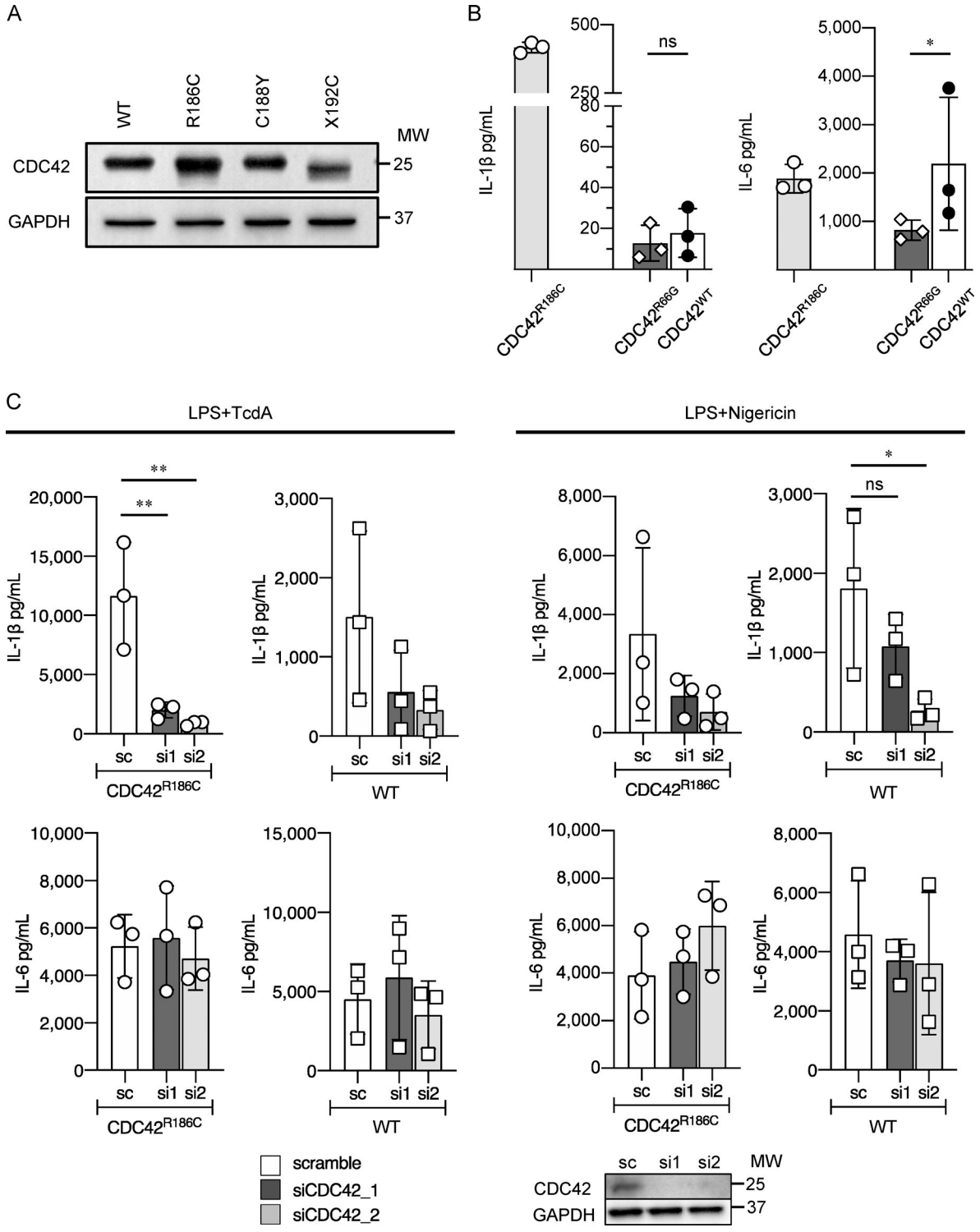

Figure S2. **Immunoblot analysis of CDC42 C-terminal variants, cytokine production from iPS-MLs carrying *CDC42*^{R66G}, and the effect of *CDC42* silencing on cytokine production from *CDC42*^{WT} and *CDC42*^{R186C} iPS-MLs. (A)** CDC42 C-terminal variants were transiently transfected into HEK293T cells, and their expression levels were evaluated by Western blot analysis. **(B)** iPSCs carrying CDC42^{R66G} were generated by manipulating WT-iPSCs by single-base editing and iPS-MPs were differentiated. Cells were stimulated with LPS + TcdA and the production of IL-1β and IL-6 was evaluated. **(C)** iPS-MLs from Patient 1 and healthy controls were treated with scramble or *CDC42* siRNA and the release of IL-1β and IL-6 was monitored in response to LPS + TcdA or LPS + nigericin stimulation. Immunoblot images at the bottom show the effects of siRNAs. Representative results of (A) two independent experiments with similar results, and (B and C) two independent experiments with three clones, are shown. Statistical significance was determined by Mann–Whitney's *U* test (B) and by Dunnet test (C). *, P < 0.05; **, P < 0.01; ns, not significant. Source data are available for this figure: SourceData FS2.

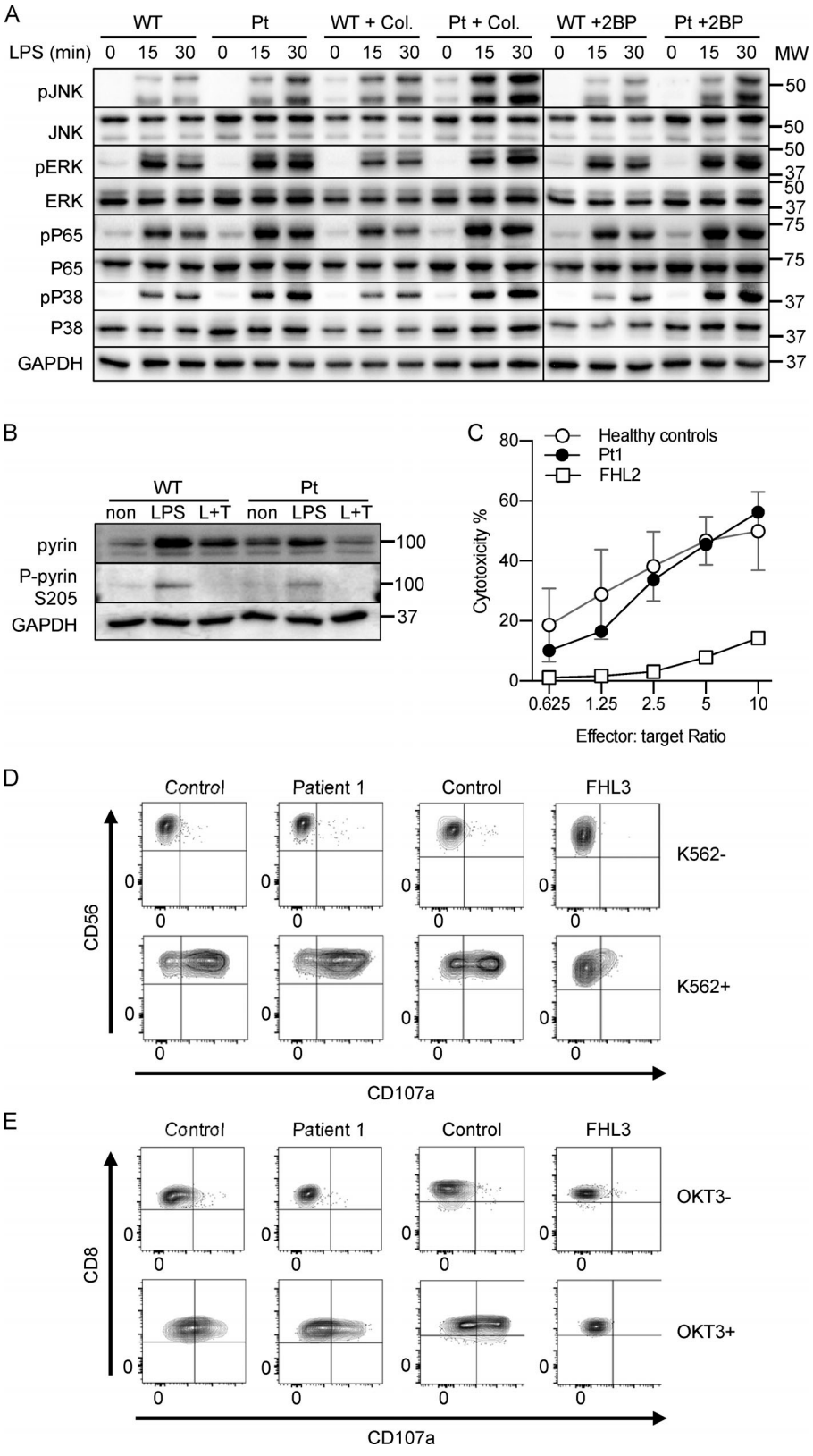

Figure S3. **Analyses of NF-κB signaling in iPS-MLs and cytolytic and degranulation activity of NK cells and CTLs from Patient 1. (A and B)** Immunoblot of JNK, ERK, P65, P38 (A) and pyrin (B) molecules and their phosphorylated forms in iPS-MLs from Patient 1 and a healthy control in response to LPS (A) and LPS ± TcdA (B) stimuli. **(C)** Cytolytic activity of activated NK cells derived from healthy controls, Patient 1, and a FHL2 patient. **(D and E)** Degranulation of activated NK cells (D) and CTLs (E) derived from healthy controls, Patient 1, and a FHL3 patient. Representative results of three (A and B) and two (C–E) independent experiments with similar results are shown. FHL, familial hemophagocytic lymphohistiocytosis. Source data are available for this figure: SourceData FS3.

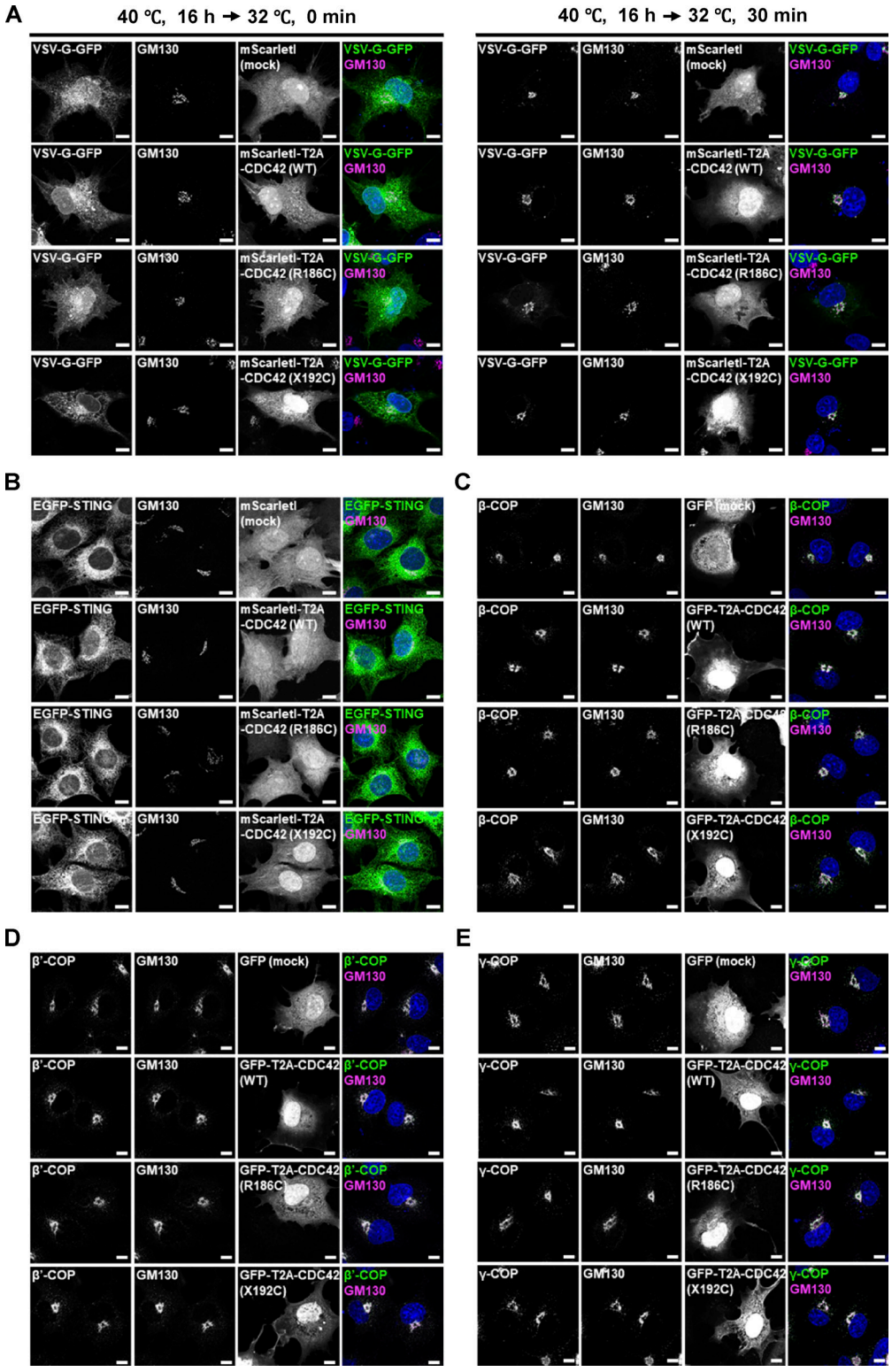

Figure S4. **CDC42^{R186C} and CDC42^{*192C*24} variants do not affect the transport and the localization of COP-I. (A)** mScarletI-T2A-CDC42 and VSV-G (tsO45)-GFP were transiently expressed in COS-1 cells. Cells were incubated at 40°C for 16 h to allow VSV-G protein to accumulate in the ER, and then at 32°C for 30 min. **(B)** mScarlet-T2A-CDC42 and EGFP-STING were stably expressed in Sting$^{-/-}$ MEFs as indicated. **(C–E)** GFP-T2A-CDC42 was transiently expressed in COS-1 cells. Cells were then fixed and stained for GM130 and for β-COP (C), β′-COP (D), and γ-COP (E). Nuclei were stained with DAPI (blue). Representative results of two independent experiments with similar results are shown. Scale bars, 10 µm.

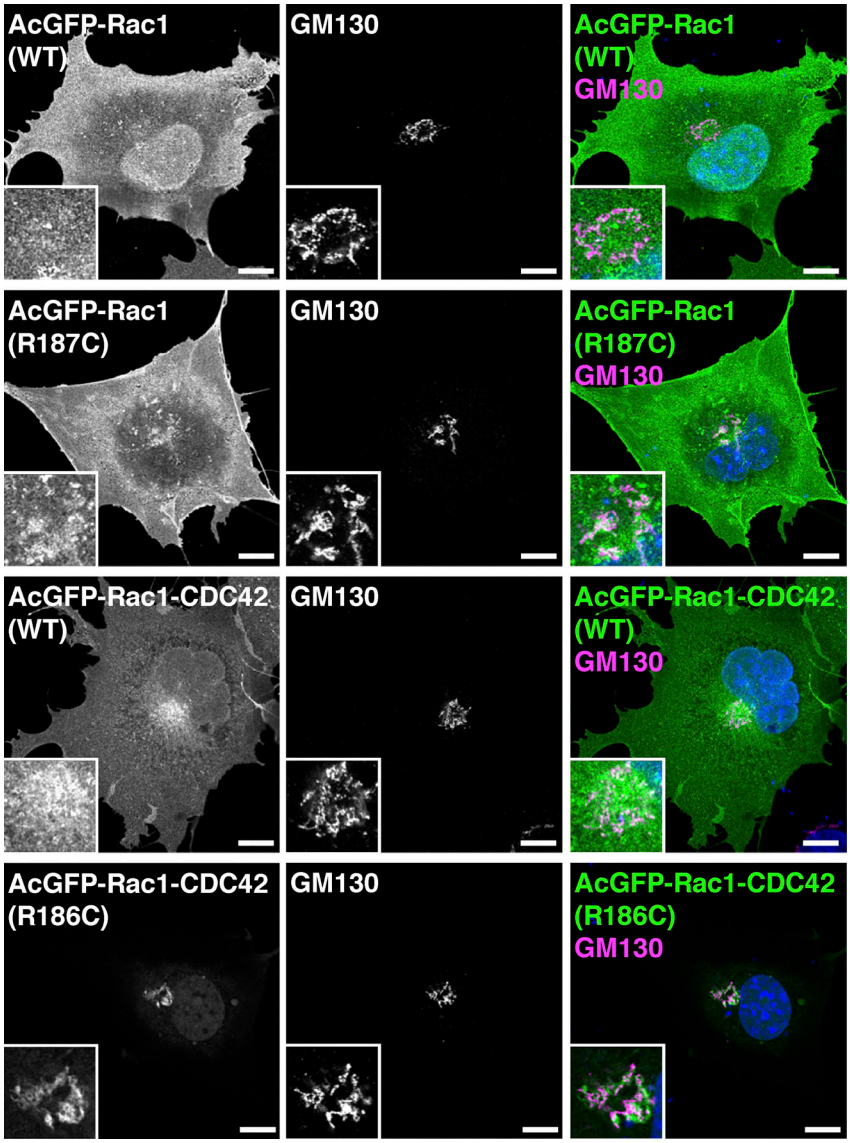

Figure S5. **Addition of the C-terminal sequence of CDC42 (R186C) to Rac1 alters its localization to the Golgi.** Rac1 or Rac1-CDC42 (C-terminal) was transiently expressed in COS-1 cells. Cells were then fixed, permeabilized, and stained for GM130. Nuclei were stained with DAPI (blue). The magnified image of the perinuclear region is shown in the lower left box. Representative results of two independent experiments with similar results are shown. Scale bars, 10 µm.